Spatial Raft Coalescence Represents an Initial Step in FcγR Signaling[1]

Hajime Kono,* Takeshi Suzuki,* Kazuhiko Yamamoto,* Masato Okada,‡ Tadashi Yamamoto,† and Zen-ichiro Honda[2]*

Characterization of lipid rafts as separated membrane microdomains consist of heterogeneous proteins suggesting that lateral assembly of rafts after Ag receptor cross-linking represents the earliest signal generating process. In line with the concept, cross-linked Ag receptors have been shown to associate with detergent-insoluble raft fraction without the aid of Src family kinases. However, it has not been established whether spatial raft coalescence could also precede Src family kinase activation. In this study, we showed that spatial raft coalescence after low-affinity FcγR cross-linking in RAW264.7 macrophages is independent of Src family kinase activity. The lateral raft assembly was found to be ascribed to the action of ligand-binding subunits, rather than to immunoreceptor tyrosine-based activation motif-bearing signal subunits, because monomeric murine FcγRIIb expressed in rat basophilic leukemia cells successfully induced spatial raft reorganization after cross-linking. We also showed that extracellular and transmembrane region of FcγRIIb is sufficient for raft stabilization. Moreover, this receptor fragment triggers rapid calcium mobilization and linker for activation of T cells phosphorylation, in a manner sensitive to Src family kinase inhibition and to cholesterol depletion. Presence of immunoreceptor tyrosine-based inhibitory motif and addition of immunoreceptor tyrosine-based activation motif to the receptor fragment abolished and enhanced the responses, respectively, but did not affect raft stabilization. These findings support the concept that ligand-binding subunit is responsible for raft coalescence, and that this event triggers initial biochemical signaling. *The Journal of Immunology*, 2002, 169: 193–203.

Receptors for Ig Fc region (FcR) belong to a family of multichain immune recognition receptors (MIRRs)[3] composed of TCR and B cell Ag receptors (BCRs) and the FcRs (1, 2). Upon the recognition of multivalent ligands or multiple MHC-peptide complexes, MIRRs trigger Src family kinase-dependent phosphorylation of tyrosine in immune receptor tyrosine-based activation motifs (ITAMs) (1, 3). Syk/Zap-70 tyrosine kinases are recruited to the ITAMs and then phosphorylate central adapter proteins such as linker for activation of T cells (LAT) or B cell linker protein (4, 5). These scaffolding proteins subsequently recruit phospholipase Cγ, Grab family proteins, and phosphatidylinositol 3-kinases, thus forming signal transduction machinery (6).

In addition to these molecular assemblies via protein-protein interactions, recent studies have revealed the significance of protein compartmentalization that relies on spatially segregated plasma membrane domain, referred to as detergent-insoluble membranes (DIM) or lipid rafts (7). Several of Src family kinases and LAT constitutively associate with lipid rafts, and TCR and FcεRI signaling is transduced solely by the raft-associating Src family members (8, 9). Clustering-dependent association of MIRRs and downstream signaling molecules with lipid rafts has been shown in a variety of systems (10–13). Upon the contact with APCs, T cells polarize to form spatially organized molecular assembly, called immunological synapse, at the contact site (14, 15). This reorganization process also uses lipid rafts as vehicles (16). Besides the roles in such late signaling events as immunological synapse formation, rafts have been claimed to function in the earliest stage of MIRR signaling. For instance, partition of FcεRI or BCR into lipid raft fractions was not prevented by the inhibition of Src family kinase activity (17, 18), and the FcεRI association with rafts was not affected by the deletion of ITAMs in β and γ subunits (19). These observations indicate that receptor-detergent insoluble membrane (DIM) association represents the earliest event after the receptor multimerization, although the mechanisms to how this process links to signal generation are still elusive.

Recent biophysical analysis of rafts showed that raft size is small enough to expect that each raft possesses different protein constituents (20). Through the pioneering studies in FcεRI system (17, 19, 21), Baird et al. (22) hypothesized that FcεRI is brought into association with Lyn after raft coalescence, and that FcεRI is then phosphorylated by Lyn. In a previous work, we showed that Lyn molecules in quiescent rat basophilic leukemia (RBL) 2H3 cells are mixture of active and inactive forms (23). Therefore, it is also possible that raft coalescence provides a field for Lyn transactivation. If the hypothesis holds, spatial raft coalescence should precede intracellular signaling. However, this problem has not

been fully examined. In this study, we first showed that FcγR-mediated spatial raft coalescence is independent of Src family kinase activity. One of the common features in receptor-DIM association is that ligand-binding subunits frequently devoid of signal-generating ITAMs actively translocate into DIM, and that signaling subunits such as FcεRI β and γ subunits, and TCR-ζ subunits are constitutively recovered from DIM (9, 12, 17). We presumed that it reflects active participation of ligand binding subunits in raft coalescence. By using monomeric FcγRIIb as a model system, we provided evidence supporting that ligand-binding subunit-mediated spatial raft coalescence represents initial and productive signaling process.

Materials and Methods
Materials

HRP-conjugated cholera toxin B (CTxB), FITC-conjugated CTxB, and methyl-β-cyclodextrin (MβCD) were from Sigma-Aldrich (St. Louis, MO). PP2 was from Calbiochem (Darmstadt, Germany). Rhodamine-conjugated streptavidin was from Molecular Probes (Eugene, OR). Protein G-Sepharose, ECL Protein Biotinylation system, and streptavidin-HRP conjugate were from Amersham Pharmacia Biotech (Buckinghamshire, U.K.). All the culture media and Geneticin were purchased from Life Tech Oriental (Osaka, Japan). FCS was from Equitec Bio (Ingram, TX). The FcεRI γ subunit knockout C57BL/6 mice (24) were purchased from Taconic Farms (Germantown, NY).

A rat anti-mouse FcγRIIb/IIIa mAb, 2.4G2, was purified from culture supernatant with protein G-Sepharose chromatography. Biotinylation of 2.4G2 and preparation of Fab were performed using ECL protein biotinylation system (Amersham Pharmacia Biotech) and immobilized papain (Pierce, Rockford, IL), respectively. FITC-conjugated 2.4G2 and FITC-conjugated rat mAb against mouse CD45 were from BD PharMingen (San Diego, CA). A mouse monoclonal anti-DNP IgE, SPE-7, was from Sigma-Aldrich. A polyclonal Ab against CTxB was purchased from Calbiochem. Anti-phosphotyrosine mAb, 4G10, was from ICN Biochemicals (Costa Mesa, CA). Polyclonal Abs against Lyn, c-Src, and Syk were from Santa Cruz Biotechnology (Santa Cruz, CA). Polyclonal Ab against LAT was from Upstate Biotechnology (Lake Placid, NY). Polyclonal Abs against rat IgG and mouse IgE were from ICN (Aurora, OH). Polyclonal Abs against FcγRIIb and common γ subunit of FcγR/FcεRI were kindly donated by Dr. T. Takai (Tohoku University, Sendai, Japan), and by Dr. R. P. Siraganian (National Institutes of Health, Bethesda, MD), respectively.

Cell culture

RAW264.7 and RBL2H3 cells were cultured as a monolayer in DMEM (Nissui Pharmaceutical, Tokyo, Japan) supplemented with 10% FCS. RAW264.7 cells stably expressing a membrane-anchored Csk (mCsk) and RBL2H3 cells stably expressing platelet activating factor (PAF) receptor (25) were described previously (9, 26).

Bone marrow cells were prepared from FcεRI γ[+/+] or γ[-/-] C57BL6 mouse, and bone marrow-derived macrophages (BMMCs) were elicited using 10% L929 cell-conditioned medium in DMEM with 10% FCS as described (27).

Preparation of RBL2H3 cells expressing FcγRIIb mutants

Truncation of murine FcγRIIb cytoplasmic domain (FcγRIIb-truncated) and replacement of the cytoplasmic domain with murine FcεRIγ subunit bearing ITAM (FcγRIIb-γITAM) were conducted as described (28). To create FcγRIIb-γ ITAM chimera, cDNAs of murine FcγRIIb2 and γ subunit were subcloned into pBlueScript II in sequence, and FcγRIIb2 extracellular and transmembrane domains were connected with γ subunit cytoplasmic domain by PCR-based techniques (28). Primers used for truncated FcγRIIb were 5'-TGGAACCTGCTTTTTCTTGA-3' and 5'-TAGTCTC CCTTGGCGAATTC-3'. Those for FcγRIIb-γ ITAM chimera were 5'-CGAAAGGCAGCTATAGCCAG-3' and 5'-TGGAACCTGCTTTTTCT TGA-3'. cDNAs were sequenced, subcloned into pCXN2 (29), and multiple RBL2H3 cell clones stably expressing wild-type (WT) and the mutated FcγRIIb were established as described (9, 30). Surface expression of WT and mutated FcγRIIbs was analyzed with flow cytometry after staining cells with FITC-conjugated 2.4G2 as described (26).

Cell stimulation and cell lysis

To stimulate cells via FcγRs, adherent RAW cells, BMMCs, or RBL cells expressing FcγRIIb or its mutants were sensitized with 2.4G2 mAb (10

μg/ml) or with 2.4G2 Fab (10 μg/ml) in ice-cold assay medium (DMEM containing 10 mM HEPES-NaOH (pH 7.4) and 1 mg/ml BSA) for 30 min. In the case of FcεRI stimulation, RBL transfectants were incubated with anti-DNP IgE (1 μg/ml) in the ice-cold assay medium for 30 min. Cells were washed twice with ice-cold assay medium, and clustering of FcγRs and FcεRI was initiated by replacing the medium with prewarmed (37°C) medium containing goat anti-rat IgG (30 μg/ml) and with DNP-BSA (100 ng/ml), respectively. After indicated periods, medium was aspirated, and cells were solubilized with 500 μl of ice cold Nonidet P-40 lysis buffer (20 mM Tris-HCl (pH 7.4), 1% Nonidet P-40, 0.1% sodium deoxycholate, 150 mM NaCl, 1 mM EDTA, 1 mM Na₃VO₄, 20 mM β-glycerophosphate, 10 μg/ml aprotinin, 5 μg/ml leupeptin, and 0.2 mM PMSF). Insoluble materials were removed by centrifugation at 12,000 rpm for 10 min at 4°C, and the supernatant was used as total cell lysate.

Immunoprecipitation and immunoblotting

Total cell lysates were first incubated with 15 μl of protein G Sepharose beads (50% slurry) to separate 2.4G2-bound materials. After continuous rotation for 1 h at 4°C, samples were centrifuged at 2500 rpm at 4°C for 2 min, and the supernatants were saved. Beads were washed three times with 500 μl of 0.1% Nonidet P-40 lysis buffer, and the 2.4G2-bound materials were eluted by boiling in 2% SDS sample buffer. The saved supernatants were incubated with various first Abs for 1 h and then with 15 μl suspension of protein G-Sepharose beads for 30 min at 4°C under continuous rotation. The beads were washed and bound materials were eluted as described above. Samples were analyzed by Western blotting using ECL detection system (Amersham Pharmacia Biotech) as described previously (9).

To analyze subunit composition of intrinsic FcεRI and transfected FcγRs in RBL cells, 1.5 × 10⁷ cells in the assay medium were sensitized with biotinylated IgE (2 μg) or with biotinylated 2.4G2 (10 μg) on ice for 60 min. Cells were lysed in 2% digitonin lysis buffer (20 mM Tris-HCl (pH 7.4), 2% digitonin, 150 mM NaCl, 1 mM EDTA, 1 mM Na₃VO₄, 20 mM β-glycerophosphate, 10 μg/ml aprotinin, 5 μg/ml leupeptin, 0.2 mM PMSF), and the receptors were immunoprecipitated with anti-mouse IgE or with anti-rat IgG and with protein G-Sepharose beads as described above.

Raft fractionation by sucrose density gradient centrifugation

Triton X-100 solubilization of cells and raft fractionation were conducted essentially following the method reported by Field et al. (17). Cell suspension at 1 × 10⁷/ml was sensitized with 2.4G2 (10 μg/ml) or with 2.4G2 Fab (10 μg/ml) in ice-cold assay medium for 30 min, washed twice and resuspended at 1 × 10⁷/ml in stimulation buffer (20 mM HEPES-NaOH (pH 7.4), 135 mM NaCl, 5 mM KCl, 1.8 mM CaCl₂, 1 mM MgCl₂, 5.6 mM glucose, 1 mg/ml BSA). Cells were prewarmed at 37°C for 5 min, challenged with goat anti-rat IgG (30 μg/ml) for indicated periods, and then solubilized by mixing with an equal volume of ice-cold 0.1% Triton X-100 lysis buffer (0.1% Triton X-100, 80 mM HEPES-NaOH (pH 7.4), 20 mM EDTA, 0.1%NaN₃, 2 mM NA₃VO₄, 20 mM β-glycerophosphate, 10 μg/ml aprotinin, 5 μg/ml leupeptin, 0.1 mM PMSF). The cell lysate was mixed with an equal volume of ice-cold 80% sucrose buffer (80% sucrose, 25 mM HEPES-NaOH (pH 7.4), 125 mM NaCl, 2 mM EDTA), and sucrose density gradients were made in 13 PA tube (1.5 × 9.6 cm; Hitachi Koki, Hitachi, Japan) by sequential layering of 0.625 ml of 80%, 1.25 ml of 60%, 3.75 ml of the cell lysate adjusted to 40% sucrose, 1.875 ml of 30%, 1.25 ml of 20%, and 1.5 ml of 10% sucrose buffers. The gradients were centrifuged at 38,000 rpm at 4°C for 18 h in RPS40T rotor (Hitachi Koki). A total of 1 ml of fractions were collected from the bottom; proteins were extracted following the methods by Wessel and Flugge (31) and analyzed by Western blotting.

Confocal microscopic analysis

Adherent RAW cells or RBL2H3 cells on Lab-Tek chamber slide (Nalge Nunc International, Rochester, NY) were first sensitized with ice-cold assay medium containing biotinylated 2.4G2 (5 μg/ml) for 30 min. In the studies to compare the distributions of FcγRs to those of CD45, FITC-conjugated anti-CD45 mAb (5 μg/ml) was also included in the medium. Cells were washed twice with ice-cold assay medium, and then treated with prewarmed (37°C) assay medium containing rhodamine-conjugated streptavidin (10 μg/ml) to initiate FcγR cross-linking. The reaction was continued at 37°C for 3 min, and terminated by the fixation of cells with of 3.7% formaldehyde in PBS. Cells were solubilized with 0.01% Triton X-100 for RAW cells or with 1% Triton X-100 for RBL2H3 cells for 3 min at room temperature, washed twice with PBS, and ganglioside GM1 and unligated FcγRs were stained with FITC-conjugated CTxB (10 ng/ml) and with rhodamine-conjugated streptavidin (10 μg/ml), respectively. Confocal

microscopic observation was performed using Zeiss LSM510 confocal microscope (Zeiss, Oberkochen, Germany) with ×63 objective lens. For excitation, a 488-nm Ar laser was used for FITC and a 543-nm HeNe laser for rhodamine. Emission band path was set at 505 nm for FITC, and at 560 nm for rhodamine.

Codistribution of FcγR with GM1 or with CD45 was quantified as described (21). The two line profiles of plasma membrane fluorescence for FITC and rhodamine were obtained from confocal images of cross sections using NIH Image (version 1.62; http://rsb.info.nih.gov/nih-image/; Ref. 32). The correlation coefficient (ρ) of the two profiles was calculated from equitation below using StatView 4.5 software (Abacus Concepts, Berkeley, CA).

$$\rho = \frac{\frac{1}{N}\sum_i^N (x_i - \langle x \rangle)(y_i - \langle y \rangle)}{\sqrt{\frac{1}{N}\sum_i^N (x_i - \langle x \rangle)^2}\sqrt{\frac{1}{N}\sum_i^N (y_i - \langle y \rangle)^2}}$$

In this equation, x_i and y_i are the intensities of FITC and rhodamine at the pixel, respectively, and $\langle x \rangle$ and $\langle y \rangle$ indicate the corresponding mean fluorescence intensities.

Copatching of CTxB with FcγRs was conducted as described by Janes et al. (33). Cells were first sensitized with biotinylated 2.4G2 Fab (5 μg/ml) and CTxB-FITC (10 μg/ml) in ice-cold assay medium for 30 min. Next, patching of CTxB was induced by the addition of anti-CTxB Ab (diluted by 1/250) in ice-cold assay medium for 30 min. Last, FcγRs were cross-linked and visualized with streptavidin-rhodamine (10 μg/ml) at 37°C for 3 min before (FcγR cross-linking (+)) or after (FcγR cross-linking (−)) cell fixation with 3.7% formaldehyde in PBS. Cell permeabilization with Triton X-100 was not applied to the copatching experiment.

Fluorometric imaging of intracellular Ca²⁺ concentration ([Ca²⁺]ᵢ)

[Ca²⁺]ᵢ was measured as described (9). Adherent cells on glass coverslips were sensitized with biotinylated 2.4G2 Fab (5 μg/ml) for 15 min or with anti-DNP IgE (1 μg/ml) for 1 h, loaded with fura-2 AM (5 μM) for 1 h at 37°C, and stimulated with streptavidin (100 nM) or DNP-BSA (100 ng/ml) in HEPES-Tyrode buffer (25 mM HEPES-NaOH (pH 7.4), 140 mM NaCl, 2.7 mM KCl, 1.8 mM CaCl₂, 12 mMNaHCO₃, 5.6 mM D-glucose, 0.49 mM MgCl₂, 0.37 mM NaH₂PO₄, 1 mg/ml BSA). Fluorometric images of cells (340/380 nm) were sequentially recorded by Argus-50 system (Hamamatsu Photonics, Hamamatsu, Japan). For presentation, 25 cells in a field were randomly assigned, and the calculated average of [Ca²⁺]ᵢ was expressed as a line graph.

Cholesterol depletion

To remove cholesterol, cells were incubated for 30 min at 37°C in the presence or absence of indicated concentrations of MβCD in HEPES-tyrode solution containing 1 mg/ml fatty acid-free BSA as described (34). For the recovery of cholesterol, cells were incubated with 2.5 mM of MβCD/cholesterol (8:1, mole/mole) complexes for 2 h at 37°C (34), or with 10% FCS in HEPES-tyrode buffer (12) for 6 h at 37°C. Total cellular cholesterol was measured using cholesterol oxidase-based assay kit (Cholesterol C-II test; WAKO, Richmond VA) after chloroform/methanol extraction of cellular lipids.

Results

FcγRIIIa and IIb association with DIM is independent of Src family kinase activity

Previous studies in FcεRI and BCR systems using Triton X-100 cell lysis followed by density gradient centrifugation technique revealed that association of oligomerized receptors with DIM is independent of intracellular signaling (17, 18). Thus, we first evaluated whether FcγRIIIa and IIb α subunits associate with DIM after the receptor cross-linking in RAW264.7 cells, and whether the receptor redistribution is independent of Src family kinase activity. FcγRIIIa and IIb α subunits were probed with biotinylated 2.4G2 mAb, cross-linked with or without second Ab, and solubilized with 0.05% Triton X-100. The total cell lysate was directly subjected to ultracentrifugation on sucrose density gradients. Fig. 1, A and B show distributions of cell surface-bound biotinylated

2.4G2, which correspond to those of FcγR-α subunits. Upon cross-linking, FcγR-α subunits became partly associated with low-density DIM fractions and codistributed with ganglioside GM1 (CTxB blot). Lyn was in part associated with DIM, and c-Src was excluded from DIM, as observed previously (Fig. 1A; Ref. 9). Fig. 1B shows the time course of FcγR-α redistribution. In this figure and in the following ones, bottom fraction (B: bottom, fraction 1 in Fig. 1A), combined soluble fractions (M: middle, factions 3–5) and combined DIM fractions (T: top, fractions 8–10) were analyzed. FcγRα subunits rapidly redistributed to DIM fraction (T) and also to bottom fraction (B) within 30 s after clustering. The receptor redistribution to the B fraction is ascribed to FcγR-α association with residual F-actin, because it was prevented by latrunculin A that depolymerize residual F-actin in vivo, but not by cytochalasin D that inhibits de novo actin polymerization (data not shown). This fraction was not further characterized in the current study. FcγR-α subunit distribution to DIM was transient; it peaked at 3 min, and declined thereafter.

To examine the roles of Src family kinase in the association of FcγR-α subunits with DIM fraction, we used Src family kinase-specific inhibitor PP2 and overexpression of gain-of-function mCsk (9, 23, 26, 30). Consistent with the observations in FcεRI and BCR systems (17, 18), clustering-induced association of FcγR-α subunits with DIM was not affected by 50 μM PP2 pretreatment or by mCsk overexpression (Fig. 1C). As shown in Fig. 1D, 50 μM PP2 pretreatment and mCsk overexpression potently suppressed tyrosine phosphorylation of three Lyn substrates, Syk, γ subunit, and FcγRIIb, to almost comparable extents. Three separate experiments using different mCsk clones yielded consistent results. These data indicate that clustering-induced FcγR-α association with DIM fraction is independent of Src family kinase activity.

Spatial raft coalescence is independent of Src kinase activity

We next examined the roles of Src family kinase activity in spatial coalescence of lipid rafts by using confocal microscopic techniques. To this end, PP2 could not be applied, because acute PP2 treatment considerably affects cell adherence to substratum. Therefore, we down-regulated Src family kinase activity by mCsk overexpression. Control RAW cells carrying vector alone or cells overexpressing mCsk adhered to Lab-Tek chamber slide were sensitized with biotinylated 2.4G2, and treated with or without rhodamine-streptavidin to cross-link FcγRs or not. Cells were fixed with formaldehyde, treated with Triton X-100 to remove detergent-sensitive materials following the methods of Janes et al. (33), and unligated FcγRs were then stained with rhodamine-streptavidin. The fixation procedures did not appreciably affect biotinylated 2.4G2 binding to streptavidin (data not shown). GM1 detected with FITC-CTxB was used as a raft marker. CD45 was regarded as a marker that is not concentrated at rafts (33).

Distributions of FcγRα subunits GM1 and CD45 before and after FcγR cross-linking were shown in Fig. 2A. As shown in the left panel, FcγRα subunits were sensitive to the detergent treatment before cross-linking and readily solubilized. After cross-linking with rhodamine-streptavidin, they accumulated as discrete Triton X-100-resistant patches along cell membrane in both control cells (WT-RAW) and in mCsk-overexpressing cells (Fig. 2A, left panel, upper row). Concurrently, coaccumulation of GM1 patches with FcγRα patches became distinguishable in control cells. Of note, formation of GM1 patches and their colocalization with ligated FcγRα subunits were well-preserved in mCsk cells, thereby indicating that suppression of Src family kinase activity did not affect lateral clustering of GM1. Almost identical results were obtained when biotinylated 2.4G2 was cross-linked with 2nd Ab
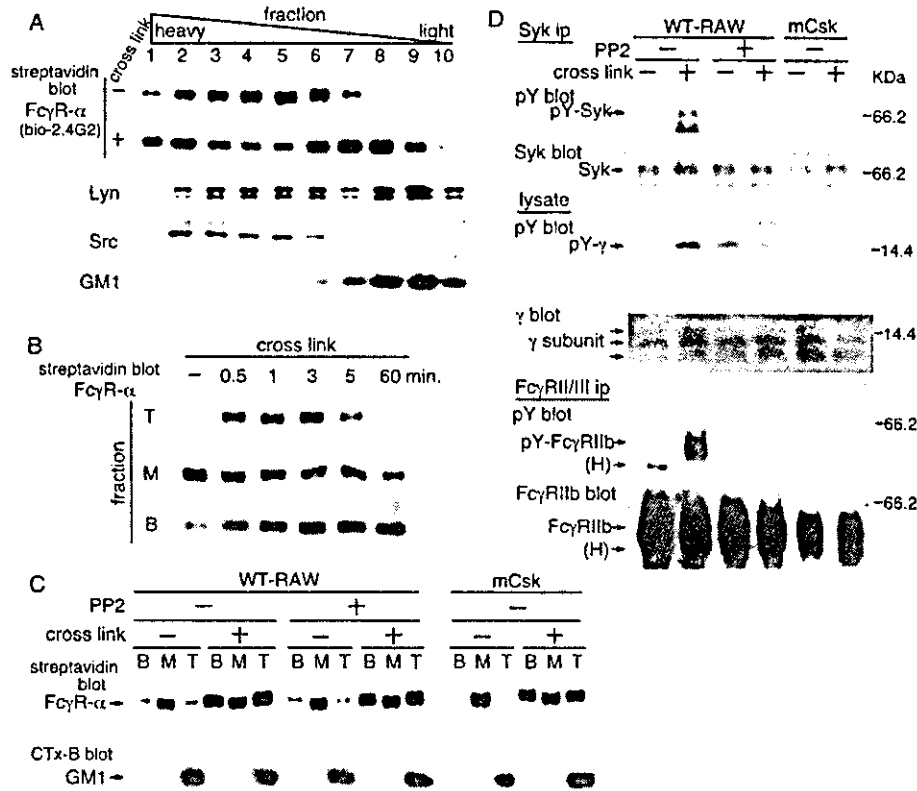
FIGURE 1. Redistribution of cross-linked FcγR to DIM. *A*, FcγRIIIa and IIb α subunits in RAW264.7 cells were probed with biotinylated 2.4G2 mAb, and cells were treated with (cross link +) or without (−) second Ab. Cells were solubilized with 0.05% Triton X-100, and subjected to sucrose density gradient centrifugation. Fractions were analyzed by Western blotting. 2.4G2-probed FcγR α subunits and GM1 were detected by HRP-streptavidin and HRP-CTxB, respectively. Blottings for Lyn, c-Src, and GM1 (CTxB blot) were those obtained from unstimulated cells. FcγR cross-linking did not alter their distributions (data not shown). *B*, Kinetics of FcγR α subunit redistribution to DIM and to the highest density fraction. In this presentation, the highest density fraction (B: bottom), combined soluble fractions (M: middle) and combined DIM fractions (T: top) are shown. *C*, Src protein tyrosine kinase (PTK)-independent FcγR α subunit redistribution to DIM. WT cells pretreated with (+) or without (−) 50 μM PP2, and mCsk-overexpressing cells were stimulated via FcγRs for 3 min, and FcγR-α redistribution was analyzed as above. PP2 and mCsk overexpression did not affect FcγR α subunit association with DIM after cross-linking. *D*, Suppression of protein tyrosine phosphorylation by PP2 treatment or by mCsk overexpression. RAW cells pretreated with (+) or without (−) 50 μM PP2, or mCsk-overexpressing cells were stimulated via FcγRs for 3 min, and tyrosine phosphorylated Syk (pY-Syk), γ-subunit (pY-γ), and FcγRIIb (pY- FcγRIIb) were analyzed by immunoprecipitation followed by Western blotting. The same membranes were reprobed with cognate first Abs after stripping. PP2 treatment and mCsk overexpression strictly suppressed these Src kinase-derived signaling.

(data not shown). As control experiments, distributions of FcγRα subunits were compared with those of CD45 (Fig. 2*A*, *right panel*). After cross-linking, FcγRα subunits again accumulated as detergent-resistant patches along cell membranes in control cells and in mCsk overexpressing cells (Fig. 2*A*, *right panel*, *upper row*). In contrast to GM1, CD45 staining along plasma membrane did not codistribute with FcγRα patches (Fig. 2*A*, *right panel*, *lower row*).

For quantitative evaluation of FcγRα subunit codistribution with GM1 and with CD45, line intensity profiles for these molecules were obtained. As shown in the representative profiles (Fig. 2*B*, *left panel*), fluorescent signals for FcγRα and GM1 were increased at discrete segments after receptor cross-linking, and these segments were clearly colocalized in both control and mCsk-overexpressing cells. Codistribution of FcγRα with GM1 was quantitatively evaluated by cross-correlation analysis (21, 32, 35). Correlation coefficient (ρ) calculated from 10 profiles for control cells and mCsk cells were significantly high (0.75 ± 0.07 and 0.70 ± 0.18, respectively). Both the values indicate matched localization of the two molecules in RBL cells (35). Almost identical results were obtained when FcγRs were cross-linked with 2.4G2 and 2nd Ab (ρ = 0.63 ± 0.07 and 0.62 ± 0.07 for WT cells and for mCsk cells, respectively; *n* = 10). Codistribution of FcγRα and CD45

was also evaluated (Fig. 2*B*, *right panel*). The intensity profiles of CD45 along plasma membrane showed nearly homogenous patterns before and after FcγR clustering. Correlation coefficients for FcγRα and CD45 after FcγR cross-linking in control cells, and mCsk cells were 0.05 ± 0.15 and 0.12 ± 0.08, respectively (*n* = 10); thus showing insignificant colocalization of these molecules (35). These data were reproducible in three separate experiments. These findings strongly suggest that coclustering of FcγRs with GM1 is not dependent on Src family kinase activity.

FcγRIIb associates with DIM in γ subunit −/− macrophages

We next tested whether ligand-binding subunits play roles in raft reorganization. To this end, monomeric FcγRIIb was used as a model system, since this receptor does not require associating subunits for cell surface expression. In addition, FcγRIIb possesses immunoreceptor tyrosine-based inhibitory motif (ITIM) in its cytoplasmic region, and FcγRIIb clustering alone does not induce tyrosine phosphorylation signaling (24, 36). These characteristics are desirable to test the hypothesis of tyrosine phosphorylation signal-independent raft coalescence.

We first examined whether cross-linking of FcγRIIb alone is sufficient for its association with DIM. BMMCs elicited from γ−/−
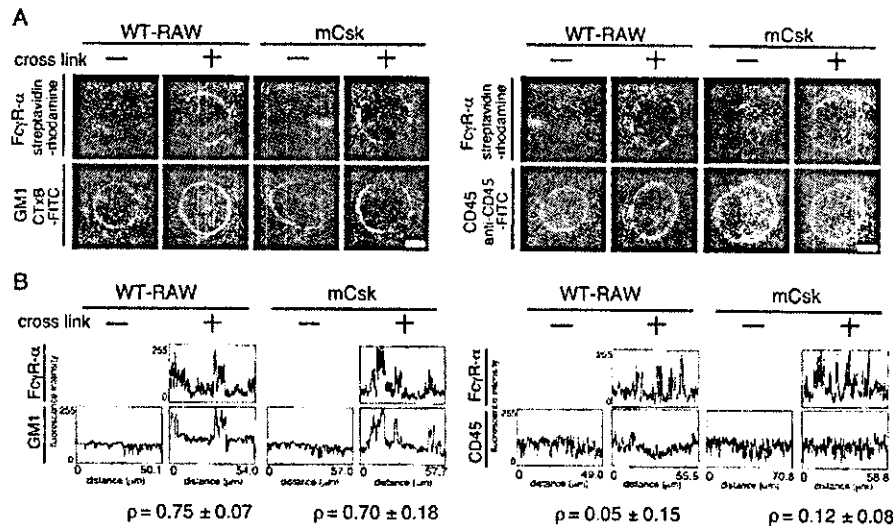
FIGURE 2. Spatial raft coalescence is independent of Src PTK activity. *A*, Analyses of spatial raft reorganization in control (WT-RAW) and mCsk-expressing RAW cells by fluorescent confocal microscopy. FcγR α subunits were probed with biotinylated 2.4G2, cross-linked (+) or not (−) with streptavidin-rhodamine for 3 min, and fixed with 3.7% formaldehyde. Cells were then solubilized with 0.01% Triton X-100. Unligated FcγR α subunits were stained with streptavidin-rhodamine after the cell fixation. GM1 and CD45 were visualized with CTxB-FITC and with FITC-conjugated anti-CD45 mAb, respectively. *Left panel*, FcγR α subunits and GM1 accumulated as discrete patches after FcγR α cross-linking in WT and mCsk-overexpressing RAW cells. *Right panel*, CD45 was almost homogenously distributed before and after FcγR α cross-linking, and did not colocalize with FcγR patches. The confocal images were taken by the identical setting in each series for comparison. The excitation/emission wavelengths were at 488/505 nm for FITC and 543/560 nm for rhodamine. Bars, 5 μm. *B*, Representative line profiles of fluorescence intensity of FcγR-α and GM1 (*left panels*), and those of FcγR-α and CD45 (*right panels*). These profiles are obtained from the confocal images in *A*. FcγR-α and GM1 signals were augmented after receptor cross-linking at discrete segments of cell membrane and these segments were colocalized in both control and mCsk-expressing RAW cells. In contrast, CD45 signal did not give detectable peaks before and after FcγR cross-linking. Codistribution of cross-linked FcγR-α with GM1 or with CD45 were quantitatively analyzed by calculating correlation coefficient (ρ) from line profiles. $\rho = 1$ corresponds to complete colocalization. The mean ± SD of ρ value was calculated from 10 individual cells.

mice were used in the experiments, because surface expression of FcγRIIIa is absent in the cells (24). FcγRIIIa and IIb on WT BMMCs or FcγRIIb on $\gamma^{-/-}$ BMMCs were probed with 2.4G2, cross-linked with or without second Ab, and changes in their distributions were examined by the raft-floating assay. As shown in Fig. 3*A*, 2.4G2 signal was increased at DIM fraction (T) after receptor clustering in WT cells, and this process was well-preserved in $\gamma^{-/-}$ cells. As shown in Fig. 3*B*, clustering of FcγRIIb alone in $\gamma^{-/-}$ cells did not induce detectable Syk tyrosine phosphorylation. These findings revealed that clustering of FcγRIIb α subunit is sufficient for its association with DIM, and the receptor redistribution is independent of tyrosine phosphorylation signaling.

*FcγRIIb extracellular and transmembrane domain is sufficient for raft reorganization*

We next studied whether monomeric FcγRIIb α could induce spatial raft reorganization, by using heterologous expression system. To test whether the presence of cytoplasmic positive (ITAM) or negative (ITIM) signal generating modules affects spatial raft reorganization, we also prepared FcγRIIb lacking almost the entire cytoplasmic region except for juxtamembrane basic cluster (aa 247–252, KKKQVP; FcγRIIb-truncated), and FcγRIIb-γ ITAM chimera, whose cytoplasmic region is replaced with that of common γ subunit possessing ITAM. Schematic representation of these structures was shown in Fig. 4*A*. These constructs were over-expressed in RBL2H3 mast cells, and multiple clones with similar expression levels of the receptors were obtained. Flow cytometric analysis of FITC-2.4G2 binding in representative cell lines and in RAW macrophages was shown in Fig. 4*B*. As compared with

RAW cells, these RBL2H3 clones expressed the FcγRIIbs at around seven times higher levels.

To exclude the unintentional association of the FcγRIIb-derived molecules with FcεRI β and γ subunits, we examined subunit composition of the FcγRIIbs by using intrinsic FcεRI as a control. Cells were sensitized with biotinylated IgE or with biotinylated 2.4G2, lysed with 2% digitonin buffer, and the receptors were isolated with corresponding second Abs. As shown in Fig. 4*C*, the IgE immunoprecipitate included β and γ subunit, as expected, whereas these subunits were nearly undetectable in 2.4G2 immunoprecipitate.

The WT and mutated FcγRIIbs were tested for their ability to associate with DIM. To this end, we used 2.4G2 Fab to probe the receptors instead of 2.4G2 whole molecule, because divalent ligation by 2.4G2 was found to induce significant translocation of the FcγRIIbs to DIM without second Ab addition (data not shown). We tentatively speculated that the premature association of dimerized receptors with DIM is due to their high expression levels. Cells sensitized with 2.4G2 Fab were treated with or without second Ab for 3 min, solubilized with 0.05% Triton X-100, and subjected to density gradient fractionation assay. As shown in Fig. 5*A*, small amounts of FcγRIIb, FcγRIIb-γ ITAM chimera, and truncated FcγRIIb were distributed at DIM fraction (T) before clustering, and the receptor cross-linking significantly augment their association with DIM.

We next compared the ability of the FcγRIIbs to spatially reorganize lipid raft. For solubilization, 1% Triton X-100 was used instead of 0.01% in these RBL clones, because the former concentration more clearly distinguished FcγRIIb and raft behaviors before and after the receptor clustering. As shown in Fig. 5*B*, FcγRIIb, FcγRIIb-γ ITAM chimera, and truncated FcγRIIb were
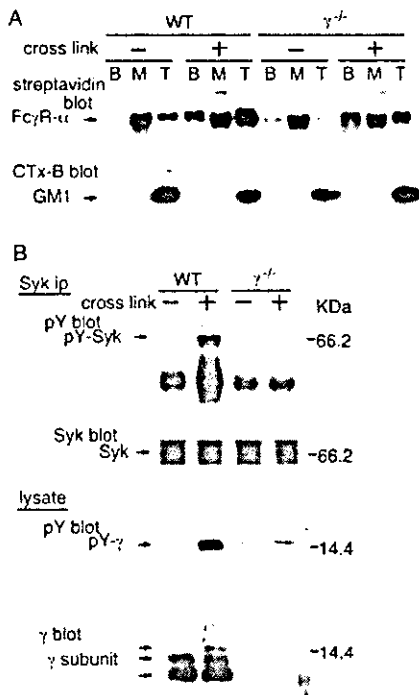
FIGURE 3. FcγRIIb redistribute to DIM after cross-linking in γ⁻/⁻ macrophages. *A*, BMMCs obtained from WT or γ⁻/⁻ C56BL/6 mice were stimulated (+) or not (−) via FcγRs, solubilized with 0.05% Triton X-100, and subjected to density gradient centrifugation assay as described in the legend for Fig. 1*B*. Cross-linking of FcγRIIb alone induced its association with DIM. *B*, Defective Syk tyrosine phosphorylation in γ⁻/⁻ macrophages. WT and γ⁻/⁻ macrophages were sensitized with 2.4G2, stimulated with (cross link (+)) or without (−) second Ab, and tyrosine phosphorylation of Syk (pY-Syk) and γ-subunit (pY-γ) were analyzed. Syk tyrosine phosphorylation was undetectable in γ⁻/⁻ macrophages.

sensitive to 1% Triton X-100 solubilization before clustering. After clustering, all the receptors acquired detergent-insolubility, and observed as prominent linear staining along plasma membrane. The homogenous distribution, instead of receptor patching observed in intrinsic FcγRs in RAW cells (see Fig. 2*A*), is presumably ascribed to the higher expression levels of the transfected FcγRIIbs. GM1 was also stabilized, and uniformly accumulated on plasma membrane after the receptor clustering. Two different sets of clones expressing the receptors yielded identical results. These findings showed that these three FcγRIIb-derived molecules possess almost identical abilities to stabilize rafts. They also showed that extracellular and transmembrane region of FcγRIIb is sufficient for raft coalescence and stabilization, and that presence of ITAM or ITIM does not influence this process.

The homogeneous distributions of the FcγRIIb-derived receptors and GM1 prevented us to assess their spatial codistributions. To confirm their colocalizations, we used raft patching study (33). GM1 was patched by FITC-conjugated CTxB and anti-CTxB Ab. The FcγRIIbs were concurrently sensitized with biotinylated 2.4G2 Fab. To cross-link the receptors, cells were treated with streptavidin-rhodamine before fixation. To visualize uncross-linked ones, streptavidin-rhodamine was added after fixation (Fig. 5*C*). As shown in the middle row of Fig. 5*C*, CTxB-FITC staining showed discontinuous, patchy distribution of GM1 along plasma membrane. In the absence of FcγRIIb-clustering, FcγRIIbs stained with streptavidin-rhodamine almost evenly distributed. After cross-linking, patchy distributions of the FcγRIIb, FcγRIIb-γ

ITAM chimera, and truncated FcγRIIb became apparent (Fig. 5*C*, *upper row*). As shown in the overlay images (Fig. 5*C*, *bottom row*), the FcγRIIbs partly codistributed with GM1 (yellow-colored segments) before the receptor cross-linking, due to their even distributions, but red-colored segments representing FcγRIIbs outside lipid rafts were clearly visible. After cross-linking, red-colored segments were almost disappeared, and discontinuous yellow patches became prominent in all the RBL transfectants. These results indicate that FcγRIIb, FcγRIIb-γ ITAM chimera, and truncated FcγRIIb almost completely colocalized with patched rafts after cross-linking.

FcγRIIb extracellular and transmembrane domain represents cell activation domain

The above findings showed that extracellular and transmembrane segment of FcγRIIb α subunit is sufficient to induce spatial raft reorganization. We subsequently tested whether this process is responsible for the generation of intracellular signaling. Fig. 6*A* shows elevation of $[Ca^{2+}]_i$ after receptor cross-linking. Control RBL cells and the cells expressing the FcγRIIbs were sensitized with biotinylated 2.4G2 Fab, challenged with streptavidin, and changes in $[Ca^{2+}]_i$ in 25 randomly assigned cells were recorded. In vector control cells and the cells expressing WT FcγRIIb, this treatment did not elicit detectable calcium mobilization. Clustering of FcγRIIb-γ ITAM chimera induced rapid and sustained $[Ca^{2+}]_i$ elevation. Of note, clustering of truncated FcγRIIb also elicited small but rapid calcium transient. As shown in the control experiments, streptavidin alone did not elicit detectable $[Ca^{2+}]_i$ elevation in the RBL2H3 clones, and clustering of intrinsic FcεRI induced almost comparable $[Ca^{2+}]_i$ elevation in the clones. These results were reproducible in two sets of RBL clones expressing the FcγRIIb-derived molecules. The peak $[Ca^{2+}]_i$ increase in two sets of clones was presented in Fig. 6*B*. The peak $[Ca^{2+}]_i$ increase was 1677 ± 44 nM and 652 ± 104 nM in cells expressing FcγRIIb-γ ITAM and truncated FcγRIIb, respectively.

We next compared clustering-induced tyrosine phosphorylation of raft-resident LAT adaptor (4, 37, 38). RBL cells sensitized with biotinylated IgE or with biotinylated 2.4G2 Fab were stimulated with streptavidin, and LAT tyrosine phosphorylation was assessed by immunoprecipitation followed by immunoblotting. As shown in Fig. 6*C*, cross-linking of FcεRI and that of FcγRIIb-γ ITAM resulted in prominent LAT tyrosine phosphorylation, whereas that of WT FcγRIIb did not induce detectable signal. Notably, cross-linking of truncated FcγRIIb elicited small but discrete LAT tyrosine phosphorylation. These findings indicate that extracellular and transmembrane segment of FcγRIIb α subunit represents cell-activating module.

We next examined by pharmacological manipulations whether the biochemical signaling elicited by truncated FcγRIIb is dependent on Src family kinase activity or on the integrity of lipid rafts. As shown in Fig. 6*D*, treatment of the cells with a Src family kinase-selective inhibitor, PP2 at 50 μM, suppressed truncated FcγRIIb-mediated peak $[Ca^{2+}]_i$ elevation by 71%, whereas this reagent did not significantly affect the response elicited by heterotrimeric G protein-coupling PAF receptor expressed in RBL cells (25, 39). PP2 treatment also decreased LAT tyrosine phosphorylation mediated by truncated FcγRIIb (Fig. 6*E*). To study the involvement of rafts in the calcium signaling, we examined the effects of cholesterol depletion by MβCD (40). As shown in Fig. 6*F*, 15 mM MβCD suppressed peak $[Ca^{2+}]_i$ elevation by 61%. Subsequent treatment of the cells with 10% FCS-containing DMEM almost completely recovered the extent of calcium response. For the recovery study, MβCD/cholesterol complex could not be applied, because addition of 2.5 mM MβCD/cholesterol complex
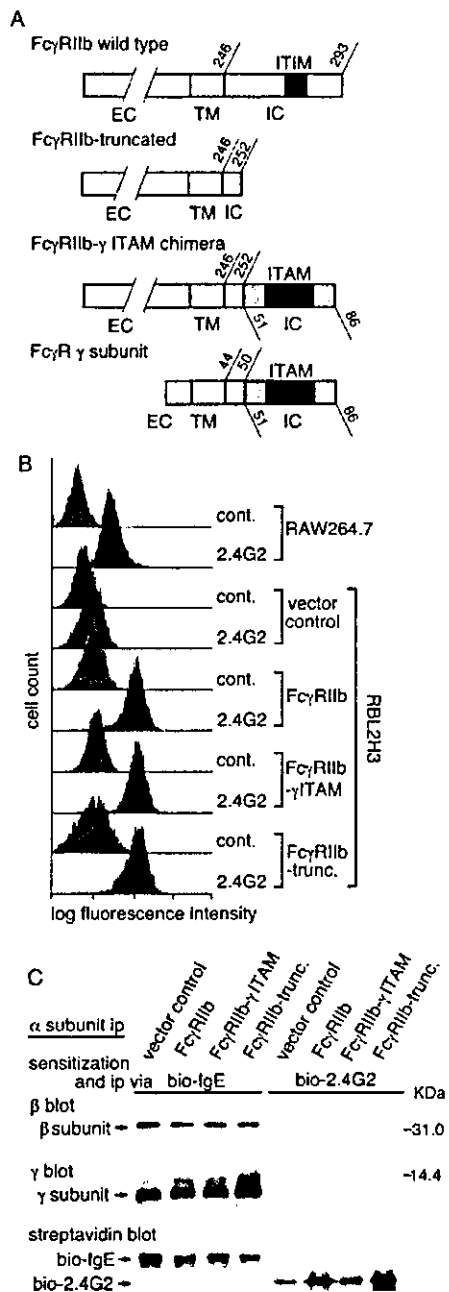
FIGURE 4. FcγRIIb and its mutated forms expressed in RBL2H3 cells. *A*, Schematic representation of murine WT FcγRIIb2, truncated FcγRIIb, and FcγRIIb-γ ITAM chimera. Structure of γ subunit is also shown. The extracellular (EC), transmembrane (TM), and intracellular (IC) domains are shown. Numbering of amino acids for FcγRIIb2 is according to Lewis et al. (49) and that of γ subunit is according to Ra et al. (50). Truncated FcγRIIb lacks almost the entire cytoplasmic region except for juxtamembrane basic cluster (247-252, KKKQVP). FcγRIIb-γ ITAM chimera was created by replacing intracellular region (253-293) of FcγRIIb with corresponding FcγR-γ subunit bearing ITAM (50-86). *B*, Analysis of surface expression of WT and the mutated FcγRIIbs expressed in RBL cells. RBL transfectants and RAW cells intrinsically expressing FcγRIIb/IIIa were stained with FITC-conjugated 2.4G2 mAb or with isotype-matched Ab. Surface fluorescence was analyzed by EPICS-XL flow cytometer (Coulter, Hialeah, FL). The expression of WT and mutated FcγRIIbs in RBL clones were almost comparable and around seven times higher than that of intrinsic FcγRIIb/IIIa in RAW cells. *C*, Lack of association of FcεRI β and γ subunits with the FcγRIIbs. RBL transfectants were sensitized with biotinylated IgE or biotinylated 2.4G2

(8/1, by mole) to MβCD-treated cells induced significant elevation of basal $[Ca^{2+}]_i$, presumably due to extensive membrane perturbation by the acute cholesterol addition (data not shown). As shown in Fig. 6*F*, MβCD at 10 and 15 mM decreased net cholesterol content to 50 and 37% of that in untreated cells, respectively, and cholesterol repletion with 10% FCS almost completely recovered the cholesterol content. Therefore, cross-linking of extracellular and transmembrane region of FcγRIIb elicits LAT tyrosine phosphorylation and calcium mobilization in a manner dependent on Src family kinase activity and on the integrity of lipid rafts. In addition, tandem ligation of ITAM and ITIM to the receptor fragment augments and suppresses the signal amplitude, respectively.

Discussion

Initiation of intracellular signaling from FcR involves conversion of physical clustering of the receptors to Src family kinase-mediated ITAM phosphorylation. Recent characterization of lipid rafts has provided a clue to consider the initial mechanisms. Findings that TCR and FcεRI signaling is catalyzed solely by raft-associating Src family kinases indicate roles of rafts in providing fields for signal generation (8, 9). It has also been shown that cross-linked FcεRI and BCR associate with DIM under the condition that intracellular signaling is suppressed (17, 18). These observations raised the possibility that receptor-DIM association represents the upstream signaling. This early process is presumed to be responsible for bringing receptors into the association with the signal initiating Src family kinases (41). This concept is well applicable to BCR system, because both surface IgM and Igα/Igβ are incorporated into DIM after clustering (13). What is apparently contradictory to the notion is that, in TCR and FcεRI systems, ITAM-bearing TCR-ζ and FcεRI β and γ subunits seems to constitutively associate with DIM, and that ligand-binding subunits lacking ITAM actively translocate into DIM after receptor clustering (9, 10, 12, 17). We presumed that this behavior of ligand-binding subunits reflects their active roles in raft coalescence. Therefore, we addressed three problems in this study. First, is spatial raft coalescence independent of Src family kinase activity? Second, are ligand-binding subunits responsible for raft reorganization? Third, does the initial raft reorganization represent productive signaling?

Although raft redistribution to the site of TCR engagements has been shown to require tyrosine kinase signaling and actin polymerization (42), it is still possible that raft reorganization in its early phase is signal-independent. We tested the first hypothesis by cytological observation of rafts after detergent treatment, following the methods by Janes et al. (33). The current findings in mCsk-overexpressing RAW cells quantitatively showed that spatial raft coalescence after FcγR clustering is independent of Src family kinase activity. These findings indicate that raft coalescence as well as FcγR association with DIM could be positioned at upstream of intracellular signaling. Signaling-independent spatial raft coalescence is further supported by efficient raft stabilization by the clustering of WT FcγRIIb ectopically expressed in RBL2H3 cells.

We next tested whether ligand-binding subunits are responsible for raft reorganization. To avoid complexity derived from associating subunits, monomeric FcγRIIb was used as a model system,

---
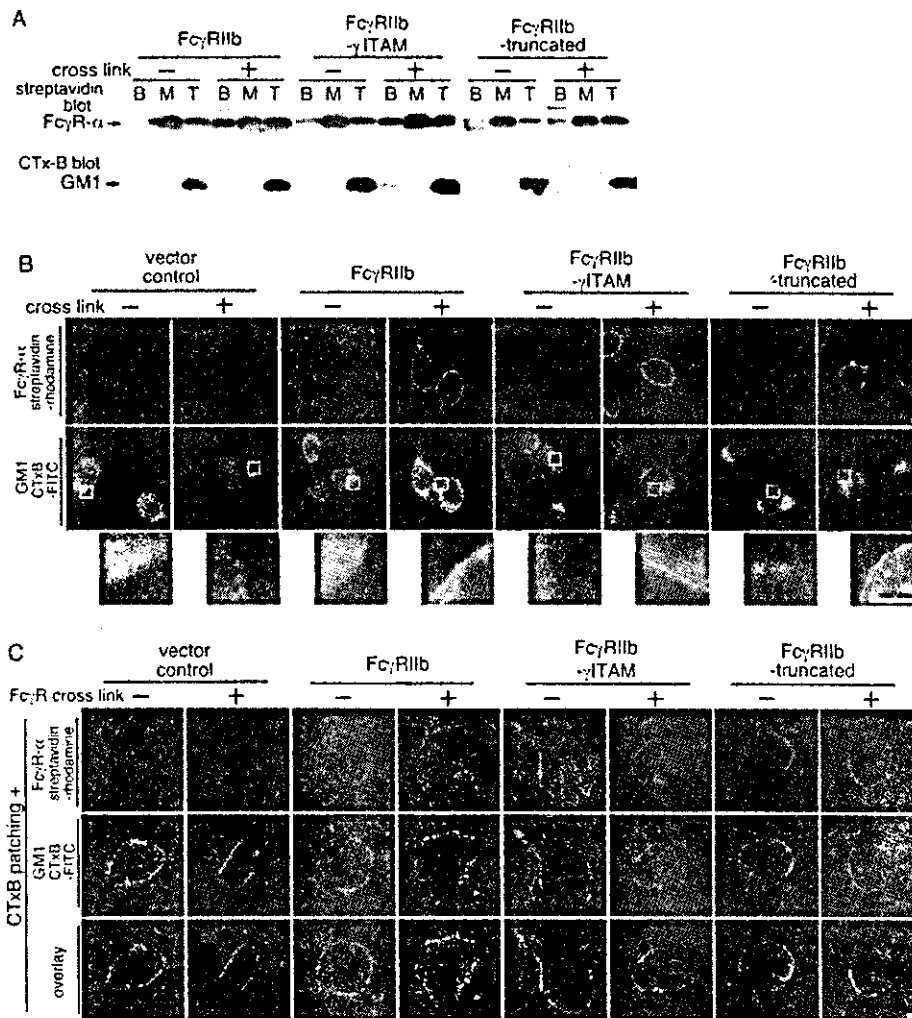
FIGURE 5. Raft reorganization by FcγRIIb and its mutated forms expressed in RBL2H3 cells. *A*, Association of the FcγRIIbs with DIM after cross-linking. The FcγRIIbs were probed with biotinylated 2.4G2 Fab, treated with (cross-link (+)) or without (−) second Ab, and association of the receptors with DIM was analyzed, as described in the legend for Fig. 1*B*. Small amounts of the FcγRIIbs were associated with DIM before clustering, but receptor cross-linking significantly enhanced the association. *B*, Raft stabilization by cross-linked FcγRIIbs. RBL2H3 cells expressing WT and mutated FcγRIIbs were treated as above, fixed with 3.7% formaldehyde, and solubilized with 1% Triton X-100 for 3 min. FcγRIIbs and GM1 were stained with streptavidin-rhodamine and CTxB-FITC, respectively, and observed by confocal microscopy. After cross-linking, all the FcγRIIbs became resistant to the detergent extraction, and accumulated along cell membrane. Rafts were also stabilized, as evidenced by clear GM1 staining at along cell membrane (see the ×6 magnified views below) after receptor cross-linking. Bars, 5 μm. *C*, Colocalization of the FcγRIIbs with patched GM1 after receptor cross-linking. GM1 was patched by incubation with CTxB-FITC and anti-CTxB Ab. The FcγRIIbs were probed with biotinylated 2.4G2 Fab, and treated with streptavidin-rhodamine before fixation (receptor cross-link (+)) or after fixation (receptor cross-link (−)) with 3.7% formaldehyde. Solubilization with Triton X-100 was not applied. *Top* and *middle rows*, The FcγRIIbs (red) and GM1 (green), respectively. In the overlay images (*bottom row*), colocalized segments of the FcγRIIbs with GM1 are yellow colored. See text for details.

because signaling subunits are frequently required for surface expression of MIRRs including FcγRIIIa, TCR, and FcεRI (2). The current findings using FcγRIIb chimeras provided an example supporting the roles of ligand-binding subunits in raft reorganization. We also showed that the extracellular and transmembrane region of FcγRIIb is sufficient for stabilizing rafts at cell membrane. Field et al. (19) showed that FcεRI α and/or γ transmembrane segment is responsible for its association with DIM fraction. The current data are consistent with their findings, and further emphasized the roles of ligand-binding subunits in spatial raft reorganization. Obviously, these findings in FcγRIIb are not sufficient to deduce general mechanisms of MIRR-mediated raft coalescence, but it is intriguing to speculate that extracellular and transmembranous segments of ligand-

binding subunits possess roles in raft reorganization besides their roles in ligand sensing.

We finally examined whether raft coalescence induced by the truncated FcγRIIb is responsible for the generation of intracellular signaling. A previous study showed that clustering of FcγRIIb alone does not lead to tyrosine phosphorylation signaling (24). We confirmed that clustering of ectopically overexpressed FcγRIIb did not induce detectable calcium mobilization or LAT tyrosine phosphorylation. We presumed that FcγRIIb-mediated raft reorganization potentially includes positive signaling, but that simultaneous ITIM condensation hindered it. Consistent with the notion, extracellular and transmembrane segment of FcγRIIb elicited discrete LAT tyrosine phosphorylation and calcium response after clustering, in a manner dependent on Src family kinase activity and on
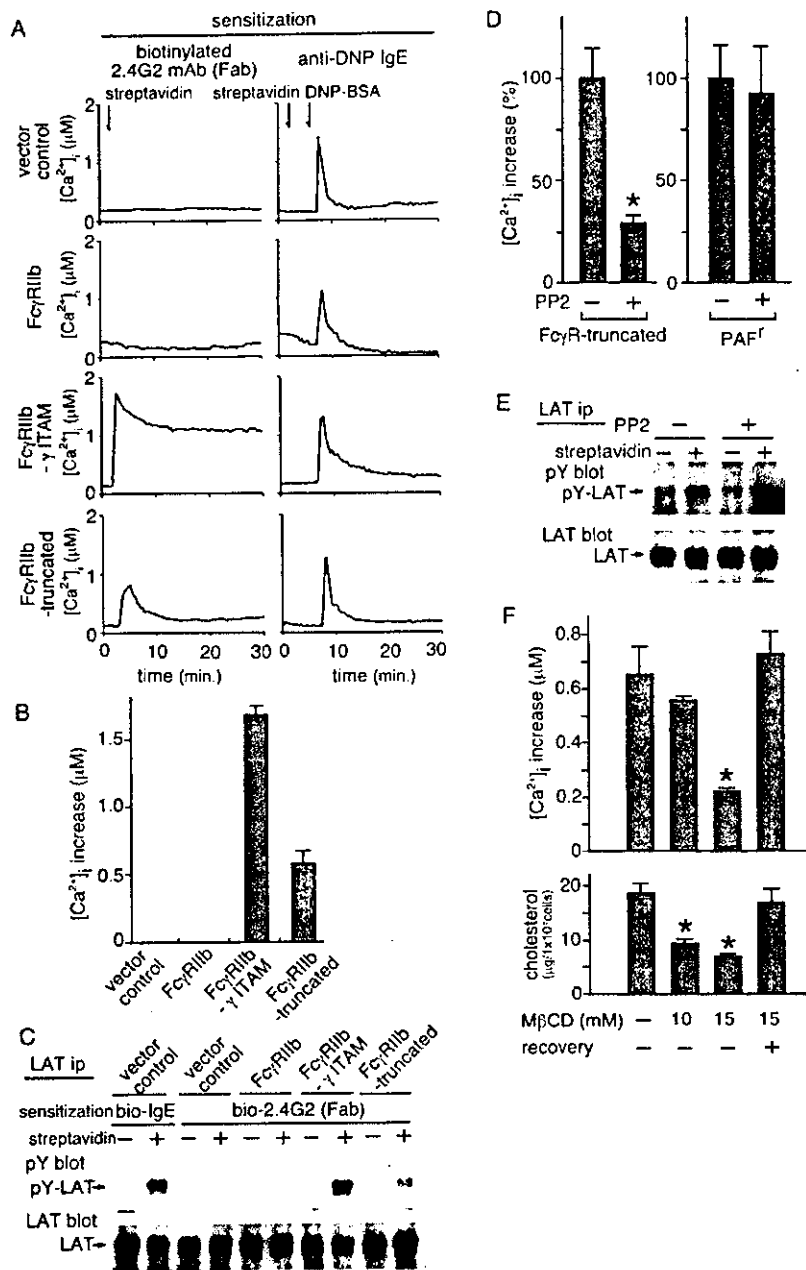
FIGURE 6. Biochemical signaling elicited by FcγRIIb and by mutated FcγRIIbs in RBL2H3 cells. *A*, Calcium mobilization in RBL2H3 cells expressing control vector, WT FcγRIIb, and mutated FcγRIIbs. RBL2H3 clones were sensitized with biotinylated 2.4G2 Fab and stimulated with streptavidin (*left panel*). The line graphs represent the average of $[Ca^{2+}]_i$ in 25 cells randomly selected. *Right panels*, The same clones were sensitized with anti-DNP IgE, and stimulated with streptavidin, subsequently with DNP-BSA Ag. *B*, $[Ca^{2+}]_i$ elevation via the FcγRIIbs in multiple clones ($n = 3$). Mean ± SD of peak $[Ca^{2+}]_i$ increase is shown. Calcium response was not detectable in control and FcγRIIb2 expressing RBL cells. FcγRIIb-γ ITAM and truncated FcγRIIb elicited $[Ca^{2+}]_i$ elevation whose peak increases were 1677 ± 44 nM and 652 ± 104 nM, respectively. *C*, Phosphorylation of LAT. The RBL2H3 clones were sensitized with biotinylated IgE or Fab of biotinylated 2.4G2, stimulated with (+) or without (−) streptavidin, and tyrosine phosphorylation of LAT (pY-LAT) were analyzed. The same membrane was reprobed with anti-LAT Ab after stripping. IgE and FcγR-γ ITAM chimera stimulation gave strong signals. Truncated FcγRIIb also induced small but discrete LAT tyrosine phosphorylation. *D*, Effects of Src PTK inhibition by PP2 on the truncated FcγRIIb-mediated calcium mobilization. RBL2H3 cells expressing truncated FcγRIIb were pretreated with 50 μM of PP2 for 30 min (+) or not (−) and stimulated via FcγR as described above ($n = 3$). RBL2H3 cells expressing PAF receptor were used as a control. PP2 suppressed peak $[Ca^{2+}]_i$ increase by 71%, whereas it marginally affected PAF-induced response. *, $p < 0.01$ compared with PP2-untreated cells by *t* test. *E*, Effects of Src PTK inhibition by PP2 on the truncated FcγRIIb-mediated LAT phosphorylation. RBL2H3 cells expressing truncated FcγRIIb were pretreated with PP2 and stimulated via FcγR as described above, and tyrosine phosphorylation of LAT (pY-LAT) was analyzed. PP2 decreased LAT tyrosine phosphorylation. *F*, Effects of cholesterol depletion on the truncated FcγRIIb-mediated calcium mobilization. RBL cells expressing truncated FcγRIIb were treated with MβCD at 0, 10, or 15 mM for 30 min, and then with (recovery +) or without (−) DMEM containing 10% FCS. Cells were stimulated as above. *Upper panel*, Peak $[Ca^{2+}]_i$ increase (mean ± SD) is presented. A total of 15 mM MβCD treatment significantly suppressed peak $[Ca^{2+}]_i$ increase by 61%, and this inhibition was reversible. *Lower panel*, The amount of cell cholesterol was determined. Ten and 15 mM MβCD treatment significantly decreased the cellular cholesterol to 50 and 37% of control, respectively, and DMEM containing 10% FCS completely restored cholesterol content. *, $p < 0.01$ compared with MβCD-untreated cells by *t* test.

raft integrity. Tandem ligation of γ ITAM to the receptor segment augmented the response. Under our experimental conditions, co-immunoprecipitation of the extracellular and transmembrane segment of FcγRIIb with γ subunit was nearly undetectable (see Fig. 4C). Although the lack of coimmunoprecipitation did not completely exclude the potential protein-protein interaction between the truncated FcγRIIb with γ subunit, the present findings support the notion that raft coalescence induced by the receptor segment triggers productive signaling. Pearse et al. (36) showed that FcγRIIb cross-linking induces B cell apoptosis, and assumed that transmembrane segment catalyzes the functions through membrane perturbation. These findings together with ours suggest significant roles of the transmembrane segment in biological functions. It could be presumed that raft reorganization is also involved in the B cell apoptosis. Obviously, the observed productive signaling by the "ITAM-less" FcγRIIb fragment does not preclude the involvement of ITAMs. It is likely that indirect condensation of ITAM-bearing subunits after raft coalescence plays roles in signal generation.

Chimera strategy as used in this study has been used to examine the roles of ITAM in MIRR signal transduction (43–45). In those studies, IL-2Rα subunit (Tac) was frequently used as a source of extracellular and transmembrane domain. Tac-γ ITAM chimeras reproducibly induced prompt signaling such as calcium mobilization or granule release, consistent with FcγRIIb-γ ITAM chimera in this study. What is apparently contradictory to our findings is that Tac constructs lacking cytoplasmic region were unable to induce early biochemical signaling (43–45). We tentatively presumed that this difference is simply due to different expression levels, but not to receptor sources, because IL-2R was shown to associate with DIM after clustering (19).

It has long been recognized that mechanical clustering of rafts by cross-linking of GPI-anchored proteins induces Src family kinase-mediated signaling (46). The current study indicates that inducible raft coalescence triggered by FcγR cross-linking could also be positioned at the upstream of Src family kinase activation, and that ligand-binding subunits are responsible for the initial process. It is also suggested that raft coalescence itself generates initial productive signaling. However, how raft coalescence leads to biochemical signaling is still undetermined. One of the possible mechanisms is that raft coalescence provides fields for one Lyn molecule to transactivate another (20). Given that that unperturbed raft is so small as estimated by biophysical analysis (20), Lyn molecules might be separated from each other. Of note, we have previously shown that Lyn molecules in RBL2H3 cells are a mixture of C-terminal tyrosine phosphorylated and dephosphorylated forms (23). Therefore, it might be possible that rafts are chimeric in terms of Lyn activity, and that the Lyn activity is dependent on the presence of Cbp/PAG-Csk complex (47, 48). As mentioned above, it is also possible that lipid rafts function as vehicles of the other signaling molecules including γ subunit, and that raft coalescence indirectly causes localized γ ITAM condensation. These possibilities should be evaluated in various model systems including γ$^{-/-}$ cells.

References

1. Weiss, A., and D. R. Littman. 1994. Signal transduction by lymphocyte antigen receptors. Cell 76:263.
2. Daeron, M. 1997. Fc receptor biology. Annu. Rev. Immunol. 15:203.
3. Cambier, J. C. 1995. Antigen and Fc receptor signaling: the awesome power of the immunoreceptor tyrosine-based activation motif (ITAM). J. Immunol. 155:3281.
4. Zhang, W., J. Sloan-Lancaster, J. Kitchen, R. P. Trible, and L. E. Samelson. 1998. LAT: the ZAP-70 tyrosine kinase substrate that links T cell receptor to cellular activation. Cell 92:83.
5. Fu, C., C. W. Turck, T. Kurosaki, and A. C. Chan. 1998. BLNK: a central linker protein in B cell activation. Immunity 9:93.
6. Tomlinson, M. G., J. Lin, and A. Weiss. 2000. Lymphocytes with a complex: adapter proteins in antigen receptor signaling. Immunol. Today 21:584.
7. Simons, K., and E. Ikonen. 1997. Functional rafts in cell membranes. Nature 387:569.
8. Kabouridis, P. S., A. I. Magee, and S. C. Ley. 1997. S-acylation of LCK protein tyrosine kinase is essential for its signalling function in T lymphocytes. EMBO J. 16:4983.
9. Honda, Z., T. Suzuki, H. Kono, M. Okada, T. Yamamoto, C. Ra, Y. Morita, and K. Yamamoto. 2000. Sequential requirements of the N-terminal palmitoylation site and SH2 domain of Src family kinases in the initiation and progression of Fcε signaling. Mol. Cell Biol. 20:1759.
10. Montixi, C., C. Langlet, A. M. Bernard, J. Thimonier, C. Dubois, M. A. Wurbel, J. P. Chauvin, M. Pierres, and H. T. He. 1998. Engagement of T cell receptor triggers its recruitment to low-density detergent-insoluble membrane domains. EMBO J. 17:5334.
11. Moran, M., and M. C. Miceli. 1998. Engagement of GPI-linked CD48 contributes to TCR signals and cytoskeletal reorganization: a role for lipid rafts in T cell activation. Immunity 9:787.
12. Xavier, R., T. Brennan, Q. Li, C. McCormack, and B. Seed. 1998. Membrane compartmentation is required for efficient T cell activation. Immunity 8:723.
13. Cheng, P. C., M. L. Dykstra, R. N. Mitchell, and S. K. Pierce. 1999. A role for lipid rafts in B cell antigen receptor signaling and antigen targeting. J. Exp. Med. 190:1549.
14. Monks, C. R., B. A. Freiberg, H. Kupfer, N. Sciaky, and A. Kupfer. 1998. Three-dimensional segregation of supramolecular activation clusters in T cells. Nature 395:82.
15. Dustin, M. L., M. W. Olszowy, A. D. Holdorf, J. Li, S. Bromley, N. Desai, P. Widder, F. Rosenberger, P. A. van der Merwe, P. M. Allen, and A. S. Shaw. 1998. A novel adaptor protein orchestrates receptor patterning and cytoskeletal polarity in T-cell contacts. Cell 94:667.
16. Viola, A., S. Schroeder, Y. Sakakibara, and A. Lanzavecchia. 1999. T lymphocyte costimulation mediated by reorganization of membrane microdomains. Science 283:680.
17. Field, K. A., D. Holowka, and B. Baird. 1997. Compartmentalized activation of the high affinity immunoglobulin E receptor within membrane domains. J. Biol. Chem. 272:4276.
18. Cheng, P. C., B. K. Brown, W. Song, and S. K. Pierce. 2001. Translocation of the B cell antigen receptor into lipid rafts reveals a novel step in signaling. J. Immunol. 166:3693.
19. Field, K. A., D. Holowka, and B. Baird. 1999. Structural aspects of the association of FcεRI with detergent-resistant membranes. J. Biol. Chem. 274:1753.
20. Pralle, A., P. Keller, E. L. Florin, K. Simons, and J. K. Horber. 2000. Sphingolipid-cholesterol rafts diffuse as small entities in the plasma membrane of mammalian cells. J. Cell Biol. 148:997.
21. Sheets, E. D., D. Holowka, and B. Baird. 1999. Critical role for cholesterol in Lyn-mediated tyrosine phosphorylation of FcεRI and their association with detergent-resistant membranes. J. Cell Biol. 145:877.
22. Baird, B., E. D. Sheets, and D. Holowka. 1999. How does the plasma membrane participate in cellular signaling by receptors for immunoglobulin E? Biophys. Chem. 82:109.
23. Honda, Z., T. Suzuki, N. Hirose, M. Aihara, T. Shimizu, S. Nada, M. Okada, C. Ra, Y. Morita, and K. Ito. 1997. Roles of C-terminal Src kinase in the initiation and the termination of the high affinity IgE receptor-mediated signaling. J. Biol. Chem. 272:25753.
24. Takai, T., M. Li, D. Sylvestre, R. Clynes, and J. V. Ravetch. 1994. FcRγ chain deletion results in pleiotrophic effector cell defects. Cell 76:519.
25. Honda, Z., M. Nakamura, I. Miki, M. Minami, T. Watanabe, Y. Seyama, H. Okado, H. Toh, K. Ito, T. Miyamoto, et al. 1991. Cloning by functional expression of platelet-activating factor receptor from guinea-pig lung. Nature 349:342.
26. Suzuki, T., H. Kono, N. Hirose, M. Okada, T. Yamamoto, K. Yamamoto, and Z. Honda. 2000. Differential involvement of Src family kinases in Fcγ receptor-mediated phagocytosis. J. Immunol. 165:473.
27. Lin, H. S., and S. Gordon. 1979. Secretion of plasminogen activator by bone marrow-derived mononuclear phagocytes and its enhancement by colony-stimulating factor. J. Exp. Med. 150:231.
28. Imai, Y., Y. Matsushima, T. Sugimura, and M. Terada. 1991. A simple and rapid method for generating a deletion by PCR. Nucleic Acids Res. 19:2785.
29. Miyazaki, J., S. Takaki, K. Araki, F. Tashiro, A. Tominaga, K. Takatsu, and K. Yamamura. 1989. Expression vector system based on the chicken β-actin promoter directs efficient production of interleukin-5. Gene 79:269.
30. Suzuki, T., S. Shoji, K. Yamamoto, S. Nada, M. Okada, T. Yamamoto, and Z. Honda. 1998. Essential roles of Lyn in fibronectin-mediated filamentous actin assembly and cell motility in mast cells. J. Immunol. 161:3694.
31. Wessel, D., and U. I. Flugge. 1984. A method for the quantitative recovery of protein in dilute solution in the presence of detergents and lipids. Anal. Biochem. 138:141.
32. Stauffer, T. P., and T. Meyer. 1997. Compartmentalized IgE receptor-mediated signal transduction in living cells. J. Cell Biol. 139:1447.

33. Janes, P. W., S. C. Ley, and A. I. Magee. 1999. Aggregation of lipid rafts accompanies signaling via the T cell antigen receptor. *J. Cell Biol. 147:447.*

34. Racchi, M., R. Baetta, N. Salvietti, P. Ianna, G. Franceschini, R. Paoletti, R. Fumagalli, S. Govoni, M. Trabucchi, and M. Soma. 1997. Secretory processing of amyloid precursor protein is inhibited by increase in cellular cholesterol content. *Biochem. J. 322:893.*

35. Pyenta, P. S., D. Holowka, and B. Baird. 2001. Cross-correlation analysis of inner-leaflet-anchored green fluorescent protein co-redistributed with IgE receptors and outer leaflet lipid raft components. *Biophys. J. 80:2120.*

36. Pearse, R. N., T. Kawabe, S. Bolland, R. Guinamard, T. Kurosaki, and J. V. Ravetch. 1999. SHIP recruitment attenuates FcγRIIB-induced B cell apoptosis. *Immunity 10:753.*

37. Zhang, W., R. P. Trible, and L. E. Samelson. 1998. LAT palmitoylation: its essential role in membrane microdomain targeting and tyrosine phosphorylation during T cell activation. *Immunity 9:239.*

38. Saitoh, S., R. Arudchandran, T. S. Manetz, W. Zhang, C. L. Sommers, P. E. Love, J. Rivera, and L. E. Samelson. 2000. LAT is essential for FcεRI-mediated mast cell activation. *Immunity 12:525.*

39. Honda, Z., T. Takano, Y. Gotoh, E. Nishida, K. Ito, and T. Shimizu. 1994. Transfected platelet-activating factor receptor activates mitogen-activated protein (MAP) kinase and MAP kinase kinase in Chinese hamster ovary cells. *J. Biol. Chem. 269:2307.*

40. Brown, D. A., and E. London. 2000. Structure and function of sphingolipid- and cholesterol-rich membrane rafts. *J. Biol. Chem. 275:17221.*

41. Cherukuri, A., M. Dykstra, and S. K. Pierce. 2001. Floating the raft hypothesis: lipid rafts play a role in immune cell activation. *Immunity 14:657.*

42. Bromley, S. K., W. R. Burack, K. G. Johnson, K. Somersalo, T. N. Sims, C. Sumen, M. M. Davis, A. S. Shaw, P. M. Allen, and M. L. Dustin. 2001. The immunological synapse. *Annu. Rev. Immunol. 19:375.*

43. Eiseman, E., and J. B. Bolen. 1992. Signal transduction by the cytoplasmic domains of FcεRI-γ and TCR-ζ in rat basophilic leukemia cells. *J. Biol. Chem. 267:21027.*

44. Letourneur, F., and R. D. Klausner. 1991. T-cell and basophil activation through the cytoplasmic tail of T-cell-receptor ζ family proteins. *Proc. Natl. Acad. Sci. USA 88:8905.*

45. Jouvin, M. H., M. Adamczewski, R. Numerof, O. Letourneur, A. Valle, and J. P. Kinet. 1994. Differential control of the tyrosine kinases Lyn and Syk by the two signaling chains of the high affinity immunoglobulin E receptor. *J. Biol. Chem. 269:5918.*

46. Stefanova, I., V. Horejsi, I. J. Ansotegui, W. Knapp, and H. Stockinger. 1991. GPI-anchored cell-surface molecules complexed to protein tyrosine kinases. *Science 254:1016.*

47. Kawabuchi, M., Y. Satomi, T. Takao, Y. Shimonishi, S. Nada, K. Nagai, A. Tarakhovsky, and M. Okada. 2000. Transmembrane phosphoprotein Cbp regulates the activities of Src-family tyrosine kinases. *Nature 404:999.*

48. Brdicka, T., D. Pavlistova, A. Leo, E. Bruyns, V. Korinek, P. Angelisova, J. Scherer, A. Shevchenko, I. Hilgert, J. Cerny, et al. 2000. Phosphoprotein associated with glycosphingolipid-enriched microdomains (PAG), a novel ubiquitously expressed transmembrane adaptor protein, binds the protein tyrosine kinase csk and is involved in regulation of T cell activation. *J. Exp. Med. 191:1591.*

49. Lewis, V. A., T. Koch, H. Plutner, and I. Mellman. 1986. A complementary DNA clone for a macrophage-lymphocyte Fc receptor. *Nature 324:372.*

50. Ra, C., M. H. Jouvin, and J. P. Kinet. 1989. Complete structure of the mouse mast cell receptor for IgE (FcεRI) and surface expression of chimeric receptors (rat-mouse-human) on transfected cells. *J. Biol. Chem. 264:15323.*

Development of TCRB CDR3 length repertoire of human T lymphocytes

Junko Nishio[1], Mihoko Suzuki[1], Toshihiro Nanki[1], Nobuyuki Miyasaka[1] and Hitoshi Kohsaka[1]

[1]Department of Bioregulatory Medicine and Rheumatology, Graduate School, Tokyo Medical and Dental University, 1-5-45 Yushima, Bunkyo-ku, Tokyo 113-8519, Japan

Abstract

The third complementarity-determining region (CDR3) of TCR interacts directly with antigenic peptides bound to grooves of MHC molecules. Thus, it is the most critical TCR structure in launching acquired immunity and in determining fates of developing thymocytes. Since length is one of the components defining the CDR3 heterogeneity, the CDR3 length repertoires have been studied in various T cell subsets from humans in physiological and pathological conditions. However, how the CDR3 length repertoire develops has been addressed only by a few reports, including one showing that CDR3 of CD4 thymocytes becomes shorter during thymic development. Here, we explored multiple regulations on the development of the TCRB CDR3 length repertoires in the thymus and the peripheral blood. CDR3 length spectratyping was employed to examine thymocyte and peripheral T cell populations for their CDR3 length repertoires. We have found that repertoire distribution patterns depend on use of the BV gene. The BV-dependent patterns were shaped during thymic selections and maintained in the peripheral blood. Differences in the mean CDR3 length among different BV subsets were seen throughout lymphocyte development. We also observed that CDR3 was shortened in both CD4 and CD8 thymocytes. Of note, the degrees of the shortening depended on the CD4/CD8 lineage and on use of the BV gene. When expansions of peripheral T cell clones are negligible, no obvious difference was seen between mature thymocytes and peripheral lymphocytes. Thus, the TCRB CDR3 length repertoires are finely tuned in the thymus before the lymphocytes emigrate into the peripheral blood.

Introduction

Using surface receptors for antigens, αβ T cells recognize antigenic peptides bound to MHC class I or II molecules. Studies using X-ray crystallography have demonstrated that three-dimensional structures composed by the first, second and third complementarity-determining regions (CDR1, 2 and 3) of TCR α and β chains interact directly with peptides presented by the MHC molecules (1,2). Avidity of the interaction is defined by topological structure and location of charged amino acid residues of the interface peptides (3). In the TCR chain, CDR3 nucleic acid sequence is most diverse because it is generated by recombination of multiple V, D (in the case of TCRβ) and J gene segments, and by random addition of interlocating N region nucleotides (4,5). Since this region interacts most closely with the antigenic peptide, the diversity of the CDR3 amino acid sequences accounts for a wide array of antigen specificities within the functional T cell repertoire.

The molecular interaction of interface peptides is similarly important in association between antigenic peptides and MHC molecules. This interaction limits heterogeneity of peptides that can bind to the products of a given MHC allele (6). The length of the antigenic peptides is also restricted by inter-action with MHC and with TCR (6). In contrast, the TCR CDR3 segments are more diverse in length. This might be explained by weaker association of antigenic peptides with TCR than with MHC (3,7). However, it remains to be seen how the CDR3 length repertoire is regulated during thymic development and in peripheral blood.

The αβ T cell repertoire develops through a number of selection steps in the thymus. TCRB gene rearrangement becomes complete first at the stage of CD3⁻CD4⁺CD8⁻ immature single-positive (CD4 ISP) thymocytes (8,9). If their TCRB genes rearrange in-frame and their products pair successfully with pre-Tα chains, these cells survive and

A

B
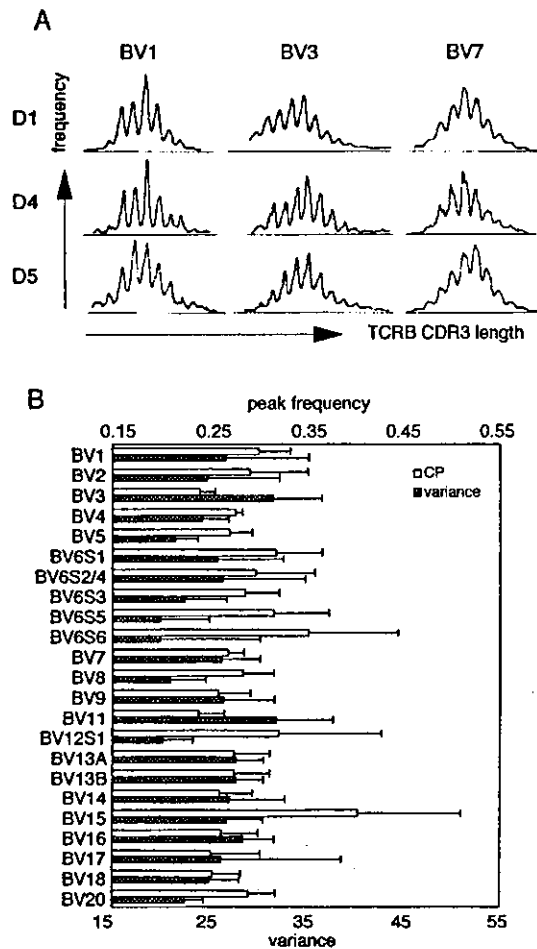
Fig. 1. BV-dependent differences in TCRB CLS histogram. (A) The histograms of the BV1, 3 and 7 subsets of peripheral CD4 T cells from three donors (D1, D4 and D5). (B) The CP frequencies and the variances in the individual BV subsets. They were calculated using TCRB CLS histograms of peripheral CD4 T cells from six child donors. The classification of the BV families was based on the definition by the WHO/International Union of Immunological Societies, Nomenclature Subcommittee on TCR Designation (30). The open columns and shaded columns represent the mean values of the CP frequencies and those of the variances respectively. The bars show their SD.

proliferate to become $CD4^+CD8^+$ double-positive thymocytes (8,10). They express TCRβ chains together with products of the in-frame rearranged TCRA gene. The double-positive thymocytes then undergo positive and negative selection, which make mature CD4 and CD8 T cell repertoires desirable to eliminate foreign pathogens. Although these processes are directed by the avidity of TCR with its ligand (11), their effects on the CDR3 length repertoire have hardly been explored.

The heterogeneity of the TCR CDR3 length in T cells at any developmental stages can be tested with TCR CDR3 length spectratyping (CLS). This method visualizes the distribution of TCR CDR3 length as histograms (12). It has been shown that typical histograms that are derived from mature peripheral T lymphocyte pools display a Gaussian-like distribution with 3-base spacing. If a histogram is biased by an unexpectedly

high frequency at a specific length, it indicates that the studied population contains an expanded T cell clone whose CDR3 has the corresponding length. Based on this, the TCR CLS technique has been employed to study clonal perturbation of T cell repertoires from healthy donors and patients with various inflammatory diseases (13–19). The results have given us some insights into the physiology and pathology of T cell homeostasis.

The above facts all indicate the importance of discerning how heterogeneity of the CDR3 length repertoire is physiologically regulated, especially in the thymus. No gross difference in CDR3 length distribution between fetal and adult T cell pools has been reported (20). Yassai *et al.* (21) reported that thymocytes with shorter TCRB CDR3 are selected during transition from $CD4^+CD8^+$ thymocytes to CD4 SP thymocytes. Their subsequent report used murine systems to show that the shortening is mediated by TCR–peptide–MHC interaction in the thymus (22). Of note, they suggested that human repertoires might be under distinct regulation. Other investigators have described that different TCRB CDR3 lengths were preferred by different BV and BJ combinations in mice (23), and BJ genes in humans (24). However, no studies have addressed which stages in lymphocyte development are responsible for these differences.

How are the CDR3 length repertoires of various T cell subsets formed, modulated and maintained in the thymus and in the peripheral blood? How does the shortening occur in the human thymus? The present study was conducted to address these issues. By examining thymocytes and peripheral T cells for TCR CLS patterns, we have found that formation of human TCR CDR3 length repertoires is under multiplex regulations in the thymus.

Methods

Samples

Thymic fragments and peripheral blood were collected from child donors during heart surgery for correction of congenital cardiac anomalies. They were from 1 to 13 years old (mean 5.6 years old). They suffered from no immunological or hematological disorders. Consent forms were obtained before the operation. CD4 ISP thymocytes, mature CD4 and CD8 SP thymocytes, and peripheral CD4 and CD8 T lymphocytes were sorted from the thymic tissues or peripheral lymphocytes as described previously (25). Purities of the separated cells were >94%.

PCR

RNA were extracted from the sorted thymocytes and lymphocytes, and converted to cDNA (25). To amplify TCR transcripts with individual TCRBV family genes, the cDNA were subjected to PCR using a fluorescent TCRBC-specific anti-sense primer ($C_\beta b$) and a panel of sense oligonucleotide primers specific to TCRBV gene families (26). The amplification reaction consisted of 35 cycles of 1 min at 94°C, 1 min at 60°C and 1 min at 72°C, with final extension at 72°C for 7 min.

To amplify TCR transcripts with individual members of the BV7 family (BV7S1, BV7S2 and BV7S3 genes), a sense primer specific to the three BV7 family genes ($V_\beta 7os$: GGA GCT CAT

GTT TGT CTA CA) and a BC-specific antisense primer [$C_\beta a$ (26)] were used for primary PCR. The reaction consisted of 25 cycles of 1 min at 94°C, 1 min at 53°C and 1 min at 72°C followed by final extension at 72°C for 7 min. Part of the products were further amplified with a nested sense primer specific to BV7S1, BV7S2 or BV7S3 genes (V_β7S1s: TAC AGC TAT GAG AAA CTC TC; V_β7S2s: TAC AGT CTT GAA GAA CGG GT; or V_β7S3s: TCT ACA ACT TTA AAG AAC AGA C) and the fluorescent $C_\beta b$ primer. The reaction consisted of 25 cycles of 1 min at 94°C, 1 min at 53°C and 1 min at 72°C followed by final extension at 72°C for 7 min.

TCR CLS

The PCR products were fractionated on denaturing 7% polyacrylamide gel in a Hitachi SQ-5500 sequencer (Hitachi Electronics Engineering, Tokyo, Japan). The data were analyzed with the associated software to display histograms. Relative percentage of the TCRB transcripts of a given length to total TCRB transcripts in the BV subsets, which is called the frequency in this report, was calculated by dividing the fluorescence intensity of the corresponding peaks by the sum of the intensity of all peaks.

Statistical analyses

CDR3 length, defined as previously described (20), ranged from 6 to 60 bases. Nineteen frequency values within this range were treated as variables for cluster analyses, which were performed with Statistica 4.1J (Tulsa, OK). The variances were calculated as follows: $\sum_{n=2}^{20} F_{3n} \times (L_{3n} - \text{mean CDR3 length})^2$, where F_{3n} stands for the frequency value that corresponds to a given CDR3 length of L_{3n}. The Kruskal–Wallis test was used to compare the central peak (CP) frequencies, variances and mean CDR3 lengths of the histograms of different BV subsets. The Mann–Whitney test was used to compare these parameters of the histograms of the CD4 ISP thymocytes with those of the other populations.

Results

BV-dependent TCRB CDR3 length repertoires of peripheral CD4 T cells

In order to characterize unbiased TCRB CDR3 length repertoires of the mature T lymphocytes, peripheral CD4 T lymphocytes from six child donors were examined. This population was studied because biases of the T cell repertoires by clonally expanded T cells are more frequent in elder individuals and in the CD8 T cell pool (13,15,27,28). Although the histogram of each BV subset displayed a Gaussian-like distribution without outstanding biases, different BV subsets had slightly different patterns. Histograms of BV1, 3 and 7 gene families of three donors are shown to represent such differences (Fig. 1A). The shapes of different BV subsets were distinguished by the height of the CP that always had the highest frequency and by the width of the span. The histograms of BV1 had a high CP and narrow span, those of BV3 had a low CP and wide span, and BV7 had modestly high CP and a narrow span.

The characteristics were quantitatively assessed with the CP frequencies and the variances; the variances indicate span of the histograms. These two values were calculated for all BV subsets studied (Fig. 1B). Various combinations of CP frequencies and variances were observed. Reflecting the histogram pattern of the BV3 subset, its CP frequencies were low and the variances were remarkably large. This was also the case with the BV11 subset. The BV1 subset, as well as the BV6S1 subset, had high CP frequencies and small variances. The two parameters also describe the characteristics of the BV7 subset: moderate CP frequency and small variance.

Although some BV subsets had higher CP frequencies than BV1, or smaller variances than BV1 and 7, the BV1, 3 and 7 subsets were further studied to investigate how these differences develop during T lymphocyte development. The other BV subsets occasionally had minor and random biases, which should be due to small expansions of T cell clones. The characteristics of the three BV subsets and similarity within the same subsets could be illuminated by line graphs of the CDR3 length repertoires from six donors (Fig. 2A). Statistical comparison of the CP frequencies and the variances among the three subsets from six donors demonstrated that the CP frequencies of the BV1 subset were highest, while those of the BV3 subset were lowest, and that the variances in the BV3 subset were largest (Fig. 3A and B).

Pannetier *et al.* (23) reported that the mean TCRB CDR3 length of murine lymphocytes depends on use of BV genes. This was the case with human peripheral lymphocytes; the mean length of the TCRBV7 transcripts was longest, while that of the TCRBV3 transcripts was shortest (Fig. 3C).

Overall differences in the CLS patterns were elucidated by cluster analysis, which treated 19 frequency values at 6–60 bases as variables. A total of 18 histograms from six donors were segregated into three groups, each of which contained histograms of BV1, 3 or 7 subsets (Fig. 4A).

According to the published database, the BV7 family consists of BV7S1, 7S2 and 7S3 genes, while BV1 and 3 families have a single gene member (29). The histograms of the BV7 subset were derived from the PCR products that were generated with a primer specific to all BV7 family genes. In order to examine the TCR transcripts with individual BV7 genes, these transcripts were independently amplified with specific primers. The CLS distributions of the transcripts with the three BV7 genes were homologous and no statistical differences in CP frequency, variance or mean TCR length were observed (data not shown). Thus, the BV7 family subset was analyzed as a whole in the present studies.

Development of the BV-dependent repertoires in the thymus

TCRBV1, 3 and 7 transcripts that were derived from CD4 ISP thymocytes, and CD4 and CD8 SP thymocytes from the same set of donors were analyzed to study how the BV-dependent characteristics develop. As was discussed in our previous report (25), the CD4 ISP thymocytes have undergone TCRB gene rearrangement, but have not started positive or negative selection. Thus, unlike CD4 CD8 double-positive cells, a part of which are already under pressure of thymic selection, they are the best for investigation of primordial TCR repertoires.

The histograms of the CD4 and CD8 SP thymocytes shared the same characteristics as those of the peripheral CD4 cells
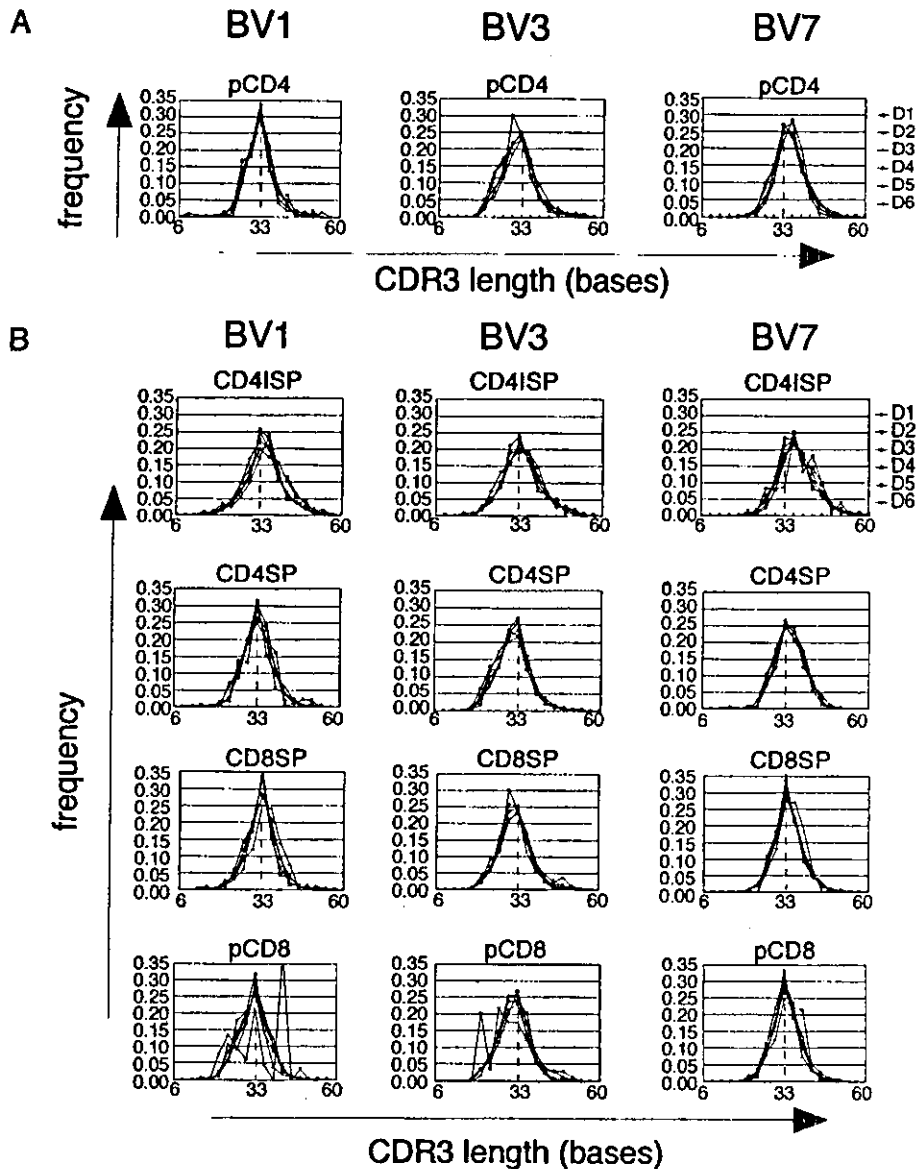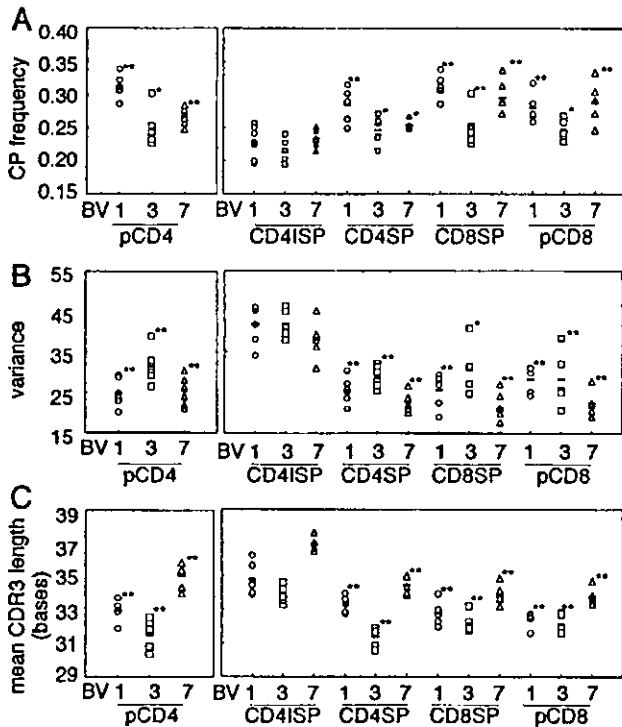
Fig. 2. TCRB CLS histograms of the BV1, 3 and 7 subsets of the peripheral lymphocytes and thymocytes. Distributions of the frequencies are presented in a line graph format. The data of the six donors (D1–D6) are shown as overlaid line graphs in each panel to illuminate BV-specific characteristics. (A) The histograms of the three BV subsets in their peripheral CD4 T cells. (B) The histograms of the CD4 ISP, CD4 SP and CD8 SP thymocytes, and peripheral CD8 T cells. Except for the CD4 ISP thymocytes, the histograms of each BV subset were similar. The BV1 and 3 subsets of the peripheral CD8 T cells from D4 were considerably biased, probably because of clonal expansions.

(Fig. 2B). In both SP populations, the CP frequencies of the BV1 subset were highest and those of the BV3 subset were lowest. The variances in the BV3 subset were largest. These differences were statistically significant (Fig. 3A and B).

Peripheral CD8 T cells from the same donors were analyzed in the same way. Their histograms were often biased since CD8 T cells are prone to large clonal expansions. Nevertheless, the BV-dependent characteristics were held well by the peripheral CD8 T cells (Figs 2B, and 3A and B).

In contrast, differences among the three subsets were not significant in the histograms of the CD4 ISP thymocytes (Fig. 2B). These histograms shared the same features, which were characterized by low CP and wide span regardless of BV gene use. In all of the three BV subsets, the CP frequencies and variances of the CD4 ISP thymocytes were different from those of the SP thymocytes and peripheral T cells in a statistically significant manner (Fig. 3A and B). The CP frequencies of CD4 ISP were significantly lower than those of CD4 SP in the BV1, 3, and 7 subsets ($P < 0.01$, $P < 0.05$ and $P < 0.05$ respectively), than those of CD8 SP ($P < 0.01$ for each subset), than those of peripheral CD4 ($P < 0.01$, $P < 0.05$ and $P < 0.01$ respectively) and than those of peripheral CD8 ($P < 0.01$, $P < 0.05$ and $P < 0.01$ respectively). The variances of CD4 ISP were significantly larger than those of CD4 SP in the

Fig. 3. Parameters to compare the TCR CLS histograms of CD4 ISP, CD4 SP and CD8 SP thymocytes, and peripheral CD4 and CD8 T cells. CP frequencies (A), variances (B) and mean CDR3 lengths (C) in the BV1, 3 and 7 subsets from the six donors are shown. Those of the peripheral CD8 T cells from D4 are excluded because of obvious biases. The Kruskal–Wallis test was used to compare the three parameters among the BV subsets. In the peripheral CD4, the three subsets were statistically different with respect to the CP frequency ($P < 0.005$), the variance ($P < 0.05$) and the mean CDR3 length ($P < 0.001$). In the CD4 ISP thymocytes, the three BV subsets were not significantly different with respect to the CP frequency and the variance, but significantly different with respect to the CDR3 length ($P < 0.002$). In the CD4 SP and CD8 SP thymocytes, the three BV subsets were different with respect to the CP frequency ($P < 0.05$ for both), the variances ($P < 0.02$ for both) and the mean CDR3 length ($P < 0.001$ and $P < 0.005$ respectively). The three BV subsets from peripheral CD8 were different with respect to the CP frequency ($P < 0.05$), the variance ($P < 0.05$) and the mean CDR3 length ($P < 0.005$). The Mann–Whitney test was used to compare the three parameters of the CD4 ISP thymocytes and the other populations. The CP frequencies of CD4 ISP were always lower than those of CD4 SP in the BV1, 3 and 7 subsets, than those of CD8 SP, than those of peripheral CD4, and than those of peripheral CD8. The variances of CD4 ISP were larger than those of CD4 SP in the BV1 3 and 7 subsets, than those of CD8 SP, than those of peripheral CD4, and than those of peripheral CD8. The mean CDR3 lengths of CD4 ISP were longer than those of CD4 SP, CD8 SP, peripheral CD4, and peripheral CD8 in all three subsets. $*P < 0.05$ and $**P < 0.01$ respectively in the Mann–Whitney test to compare each T cell population with the corresponding CD4 ISP population.

BV1, 3 and 7 subsets ($P < 0.01$ for each subset), than those of CD8 SP ($P < 0.01$, $P < 0.05$, and $P < 0.01$ respectively), than those of peripheral CD4 ($P < 0.01$ for each subset) and than those of peripheral CD8 ($P < 0.01$ for each subset).

As for the mean CDR3 length, the same differences among the three BV subsets were observed in the CD4 and CD8 SP thymocytes, and in the peripheral CD8 T cells (Fig. 3C). Unlike the distribution patterns, the differences in length were already

seen in the CD4 ISP thymocytes (Fig. 3C). These results imply that positive and negative selections exert distinct effects on CLS distribution pattern and on CDR3 length.

Cluster analyses segregated the histograms of the CD4 and CD8 SP thymocytes into three groups, each of which contained primarily those of the same BV subset (Fig. 4C and D). The histograms of the peripheral CD8 T cells also fell into the three groups except for the histograms with biases (Fig. 4B). Notably, the same analysis of the histograms of the ISP thymocytes failed to discriminate BV gene use (Fig. 4E). This should be due to similarity of the distribution patterns and suggests that the difference in length alone is not enough for segregation.

### BV- and co-receptor-dependent shortening of TCRB CDR3 length in the human thymus

It has been reported that TCR CDR3 shortens during transition from the ISP thymocytes to the SP thymocytes (21). This was observed in our studies of the mean CDR3 length; the CD4 ISP thymocytes had longer CDR3 than the other populations (Fig. 3C). To investigate this further, we analyzed plots of differences in frequency (ΔF) and skew values ($\Sigma \Delta F$), both of which have been defined by Yassai et al. (21,22). ΔF can be calculated by subtracting the CLS frequency of a given population from that of the other at the same length. A cluster of positive ΔF values on the right of an inflection point with a corresponding cluster of negative ΔF values on the other side indicates that the given population has shorter CDR3. $\Sigma \Delta F$ is the sum of ΔF values to the right of the inflection points. The ΔF plots and $\Sigma \Delta F$ were calculated by subtraction of the frequencies of the CD4 and CD8 SP thymocytes from those of the CD4 ISP thymocytes in the three BV subsets (Fig. 5A). Their patterns and positive $\Sigma \Delta F$ values showed that both SP thymocyte populations had shorter CDR3 than the CD4 ISP thymocytes irrespective of BV subset.

Interaction of TCR with endogenous antigens dictates CD4/CD8 lineage commitment during positive and negative selections in the thymus. This led us to assume that the shortening could be a function of the lineage if it is a consequence of TCR triggering. We then calculated ΔF between cells with different lineages; between the CD4 and CD8 SP thymocytes and between the peripheral CD4 and CD8 T cells (Fig. 5B). The ΔF plots and $\Sigma \Delta F$ showed that the TCR CDR3 length of CD4 lineage cells was shorter in the BV3 subset, whereas it was longer in the BV7 subset. No significant differences in CDR3 length were seen in the BV1 subset. Thus, differential shortening between CD4 and CD8 lineage cells was observed and it depended on BV gene use.

Additionally, the CD4 SP thymocytes and the peripheral CD4 T lymphocytes, as well as the CD8 SP thymocytes and the peripheral CD8 T lymphocytes, were compared. The results showed that CDR3 of CD4 or CD8 lineage cells do not shorten in the peripheral blood (data not shown).

Discussion

The present study has elucidated how TCR CDR3 length repertoires of CD4 and CD8 T cells in different BV subsets develop in the human thymus and peripheral blood. The CDR3 length repertoires had BV-dependent distribution patterns.
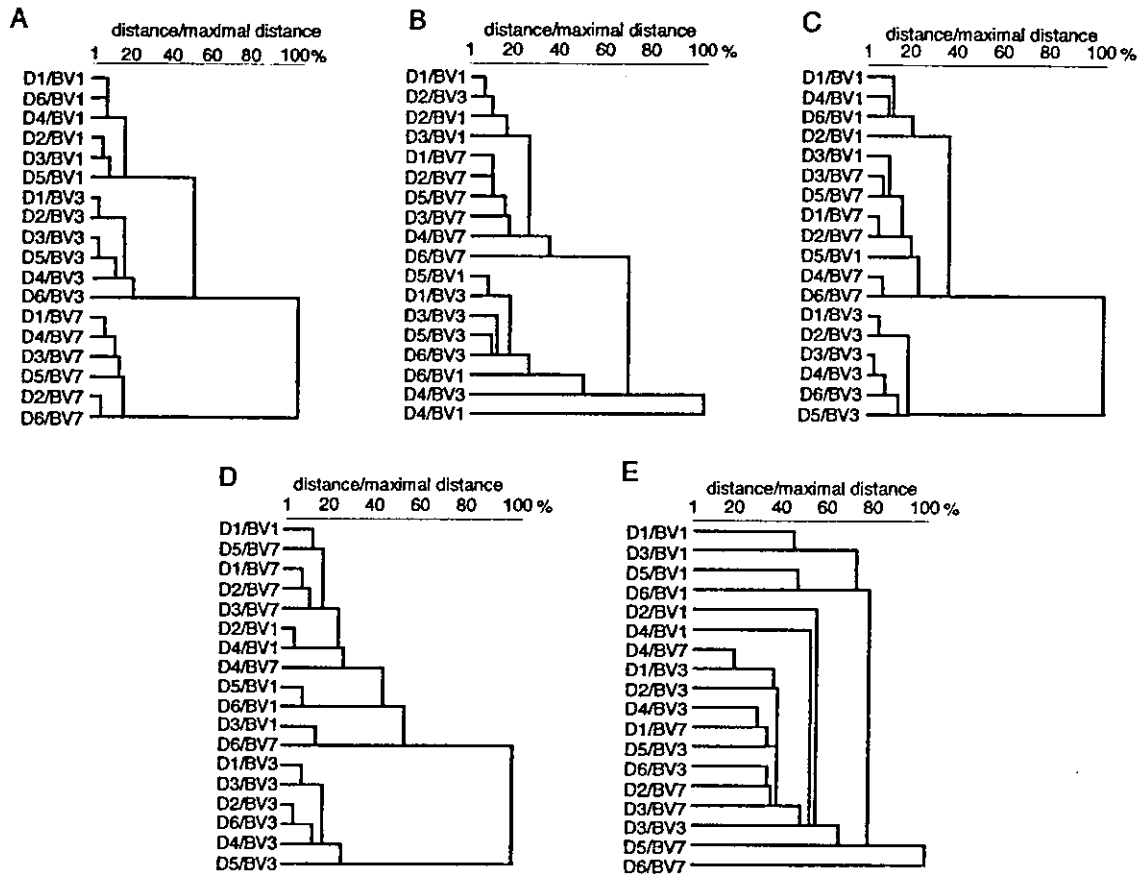
Fig. 4. Cluster analyses of the histograms of individual T cell populations from the six donors. Based on 18 histograms of peripheral CD4 (A) and CD8 (B) T cells, CD4 SP (C) and CD8 SP (D) thymocytes, and CD4 ISP thymocytes (E), the distance of every combination of two histograms was calculated with Ward's method and the Euclidean distance. All calculated distances divided by the maximal distance are shown in a dendrogram. Listed on the left are the BV subsets and the identification of donors that the individual histograms originated from. The BV1 and 3 subsets of the peripheral CD8 T cells from D4 had biased CLS histograms.

They were shaped during thymic selections and maintained in the peripheral blood. In contrast, the BV-dependent differences in the TCR CDR3 length were observed throughout lymphocyte development. The CDR3 became shorter during thymic selections, but did not change the BV-dependent differences seen before the selections. Finally, the degrees of the shortening differed between CD4 and CD8 lineage cells, and also were dependent on BV gene use. The repertoires of peripheral lymphocytes reflected directly those of mature SP thymocytes except for biases induced by clonal expansions.

Although it was known that different CDR3 lengths were preferred by different BV subsets, the BV-dependent distribution patterns are disclosed here for the first time. Unlike the difference in length, the different patterns become evident during positive and negative selections, accompanied by an increase of the CP frequency and narrowing of the distribution span. This argues that they are shaped under the pressure of positive and negative selections in the thymus. Most studies that employed the TCR CLS technique disregarded the differences, probably because the technique was used for identification of gross changes.

We have found that the distribution patterns of three gene members of the BV7 family shared the same characteristics. This ensures that the CLS histograms generated with the primer specific to BV7 family genes were not artifacts. In this regard, we have found that different gene members of the BV6 family could have similar distribution patterns (Fig. 1B). Also, both BV3 and 11 subsets shared histograms with low CP frequencies and large variances. Arden *et al.* (29) pointed out that these two genes are closely related both structurally and in their CDR3 sequences. According to their TCRBV gene classification, BV1, 3 and 7 fall into different groups. These facts argue that the BV-dependent differences could be attributable to the structure of TCRβ chains.

Using murine thymus, Pannetier *et al.* (23) observed that different BV subsets prefer different TCR CDR3 lengths. We found that the BV-dependent difference in mean TCR length already occurred in the CD4 ISP thymocytes. This implies that the difference is regulated by TCR rearrangement. Also, since the CD4 ISP thymocytes with complete TCRB gene rearrangement are under pressure of subsequent β selection for association with pre-Tα chains, the β selection could contribute to the difference formation. Moreover, the CLS histograms

A

B
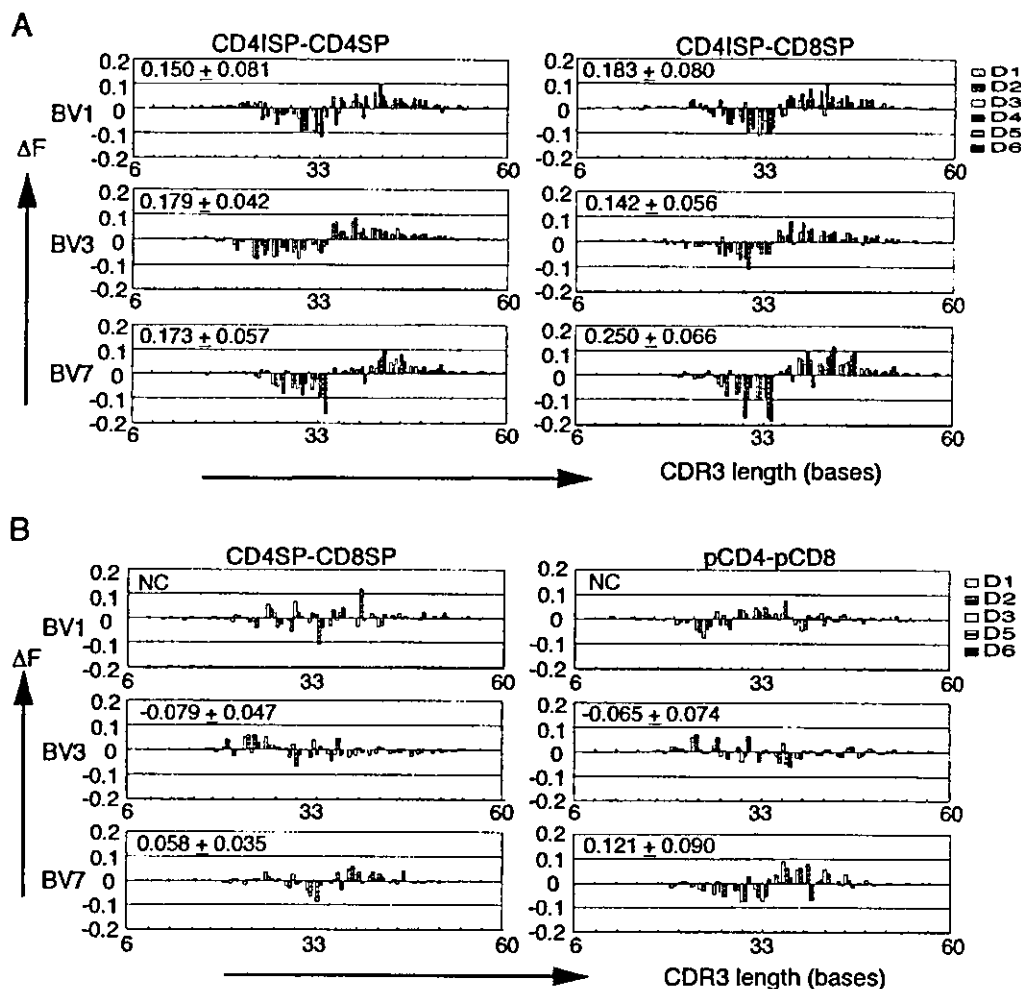
Fig. 5. Comparison of TCR CDR3 length in different CD4/CD8 lineage cells. Plotted are ΔF that were calculated by subtracting the frequencies in the CD4 and CD8 SP thymocytes from those in the ISP thymocytes (A: CD4 ISP – CD4 SP and CD4 ISP – CD8 SP respectively), and by subtracting the frequencies in the CD8 SP thymocytes from those in the CD4 SP thymocytes and those in the peripheral CD8 T cells from those in the peripheral CD4 T cells (B: CD4 SP – CD8 SP and peripheral CD4 – peripheral CD8 respectively). In order to quantify the shortening, the means ± SD of ΣΔF derived from the six donors were calculated (shown in the panels). In (B), where the data from D4 have been excluded, ΣΔF values of the BV3 subsets were all negative in both subtractions, while ΣΔF values of the BV7 subsets were all positive. ΣΔF values were not calculated for the BV1 subset because no inflection points were found in the ΔF plots. NC, not calculated.

of the BV1, 3 and 7 subsets of the CD4 ISP thymocytes were similar, but not necessarily identical (Fig. 2B), suggesting that the rearrangement and/or β selection may have a subsidiary effect in shaping the CLS distribution patterns.

To address further if the rearrangement *per se* regulates the BV-dependent difference in CDR3 length, we tried to amplify non-productively recombined TCRBV1, 3 and 7 genes from peripheral T lymphocytes that do not express TCRVβ1, 3 or 7. However, even from >10⁷, a sufficient amount of the rearranged genes could not be amplified for the TCR CLS analyses. This was consistent with the fact that the TCRB CLS patterns of the CD4 ISP thymocytes always had 3-base pair spacing, indicating that all transcripts were in-frame. The 3-base spacing was also observed by Yassai *et al.* (21) who examined TCRB genomic DNA derived from the same population. It is known that 85% of CD4 ISP thymocytes retain

the TCRB germline configuration, while only 5% express rearranged TCRB gene products (9). Thus, thymocytes with out-of-frame TCRB rearrangements must be diluted out quickly by those expressing complete TCRβ/pre-Tα and become undetectable with conventional technologies.

In separate experiments, we have assessed the mean TCR CDR3 lengths of the other BV subsets and found that the BV subsets with similar CLS patterns do not necessarily have similar CDR3 length (data not shown). The differences in shortening between CD4 and CD8 lineage cells were not a function of the distribution patterns (data not shown). Thus, distribution pattern and length appeared to be regulated independently.

Yassai *et al.* (21,22) reported TCR shortening in the human and murine thymi. By examining murine thymocytes for the BV1–BJ2 recombinants, they have shown that the shortening

occurs to a larger extent in the CD4 lineage cells than in the CD8 lineage cells. They failed to see differential shortening in humans and suggested a distinct regulation for human thymocytes. However, we observed a clear difference between the CD4 and CD8 T cells. We found that the differential shortening was a function of BV gene use. These data imply that the shortening in humans is regulated by antigen recognition by TCR.

The TCR shortening could be affected by allelic variations of MHC gene products, and differential shortening between CD4 and CD8 lineage cells could be due to differential orthogonal geometry of TCR and antigenic peptide in the grooves of MHC class I and II molecules (22). However, the differences in mean CDR3 length were preserved throughout the thymic selections. The CD4 and CD8 lineage cells share the same CLS distribution patterns. Thus, although limitations in sample collection did not allow us to investigate the effects of HLA variations, the geometry should not be the only factor regulating CDR3 length repertoire.

Development of the TCRB CDR3 length repertoire is regulated delicately in the thymus. Peripheral selections have little effect unless T cell clones expand massively in response to immunological insults. Elucidation of these thymic regulations may shed more light on molecular interaction of TCR with self-peptide–MHC in the thymus.

Acknowledgements

Abbreviations

ΔF	differences in frequency
ΣΔF	skew value
CDR	complementarity-determining region
CLS	CDR3 length spectratyping
CP	central peak
ISP	immature single positive
SP	single positive

References

1 Garboczi, D. N., Ghosh, P., Utz, U., Fan, Q. R., Biddison, W. E. and Wiley, D. C. 1996. Structure of the complex between human T-cell receptor, viral peptide and HLA-A2. *Nature* 384:134.

2 Garcia, K. C., Degano, M., Stanfield, R. L., Brunmark, A., Jackson, M. R., Peterson, P. A., Teyton, L. and Wilson, I. A. 1996. An αβ T cell receptor structure at 2.5 Å and its orientation in the TCR–MHC complex. *Science* 274:209.

3 Jorgensen, J. L., Reay, P. A., Ehrich, E. W. and Davis, M. M. 1992. Molecular components of T-cell recognition. *Annu. Rev. Immunol.* 10:835.

4 Wilson, R. K., Lai, E., Concannon, P., Barth, R. K. and Hood, L. E. 1988. Structure, organization and polymorphism of murine and human T-cell receptor α and β chain gene families. *Immunol. Rev.* 101:149.

5 Davis, M. M. 1990. T cell receptor gene diversity and selection. *Annu. Rev. Biochem.* 59:475.

6 Rammensee, H. G. 1995. Chemistry of peptides associated with MHC class I and class II molecules. *Curr. Opin. Immunol.* 7:85.

7 Matsushita, S., Takahashi, K., Motoki, M., Komoriya, K., Ikagawa, S. and Nishimura, Y. 1994. Allele specificity of structural requirement for peptides bound to HLA-DRB1*0405 and -DRB1*0406 complexes: implication for the HLA-associated susceptibility to methimazole-induced insulin autoimmune syndrome. *J. Exp. Med.* 180:873.

8 Ramiro, A. R., Trigueros, C., Marquez, C., San Millan, J. L. and Toribio, M. L. 1996. Regulation of pre-T cell receptor (pTα-TCRβ) gene expression during human thymic development. *J. Exp. Med.* 184:519.

9 Blom, B., Verschuren, M. C., Heemskerk, M. H., Bakker, A. Q., van Gastel-Mol, E. J., Wolvers-Tettero, I. L. M., van Dongen, J. J. M. and Spits, H. 1999. TCR gene rearrangements and expression of the pre-T cell receptor complex during human T-cell differentiation. *Blood* 93:3033.

10 Fehling, H. J., Krotkova, A., Saint-Ruf, C. and von Boehmer, H. 1995. Crucial role of the pre-T-cell receptor α gene in development of αβ but not γδ T cells. *Nature* 375:795.

11 Sebzda, E., Mariathasan, S., Ohteki, T., Jones, R., Bachmann, M. F. and Ohashi, P. S. 1999. Selection of the T cell repertoire. *Annu. Rev. Immunol.* 17:829.

12 Pannetier, C., Even, J. and Kourilsky, P. 1995. T-cell repertoire diversity and clonal expansions in normal and clinical samples. *Immunol. Today* 16:176.

13 Hingorani, R., Choi, I. H., Akolkar, P., Gulwani, A. B., Pergolizzi, R., Silver, J. and Gregersen, P. K. 1993. Clonal predominance of T cell receptors within the CD8+ CD45RO+ subset in normal human subjects. *J. Immunol.* 151:5762.

14 Gorski, J., Yassai, M., Zhu, X., Kissela, B., Keever, C. and Flomenberg, N. 1994. Circulating T cell repertoire complexity in normal individuals and bone marrow recipients analyzed by CDR3 size spectratyping. Correlation with immune status. *J. Immunol.* 152:5109.

15 Schwab, R., Szabo, P., Manavalan, J. S., Weksler, M. E., Posnett, D. N., Pannetier, C., Kourilsky, P. and Even, J. 1997. Expanded CD4+ and CD8+ T cell clones in elderly humans. *J. Immunol.* 158:4493.

16 Maccalli, C., Farina, C., Sensi, M., Parmiani, G. and Anichini, A. 1997. TCR β-chain variable region-driven selection and massive expansion of HLA-class I-restricted antitumor CTL lines from HLA-A*0201+ melanoma patients. *J. Immunol.* 158:5902.

17 Lin, M. Y. and Welsh, R. M. 1998. Stability and diversity of T cell receptor repertoire usage during lymphocytic choriomeningitis virus infection of mice. *J. Exp. Med.* 188:1993.

18 Sourdive, D. J., Murali, K. K., Altman, J. D., Zajac, A. J., Whitmire, J. K., Pannetier, C., Kourilsky, P., Evavold, B., Sette, A. and Ahmed, R. 1998. Conserved T cell receptor repertoire in primary and memory CD8 T cell responses to an acute viral infection. *J. Exp. Med.* 188:71.

19 Nishio, J., Suzuki, M., Miyasaka, N. and Kohsaka, H. 2001. Clonal biases of peripheral CD8 T cell repertoire directly reflect local inflammation in polymyositis. *J. Immunol.* 167:4051.

20 Moss, P. A. and Bell, J. I. 1995. Sequence analysis of the human αβ T-cell receptor CDR3 region. *Immunogenetics* 42:10.

21 Yassai, M. and Gorski, J. 2000. Thymocyte maturation: selection for in-frame TCR α-chain rearrangement is followed by selection for shorter TCR β-chain complementarity-determining region 3. *J. Immunol.* 165:3706.

22 Yassai, M., Ammon, K., Goverman, J., Marrack, P., Naumov, Y. and Gorski, J. 2002. A molecular marker for thymocyte-positive selection: selection of CD4 single-positive thymocytes with shorter TCRB CDR3 during T cell development. *J. Immunol.* 168:3801.

23 Pannetier, C., Cochet, M., Darche, S., Casrouge, A., Zoller, M. and Kourilsky, P. 1993. The sizes of the CDR3 hypervariable regions of the murine T-cell receptor β chains vary as a function of the recombined germ-line segments. *Proc. Natl Acad. Sci. USA* 90:4319.

24 Hall, M. A. and Lanchbury, J. S. 1995. Healthy human T-cell receptor β-chain repertoire. Quantitative analysis and evidence for J β-related effects on CDR3 structure and diversity. *Hum. Immunol.* 43:207.

25 Nanki, T., Kohsaka, H. and Miyasaka, N. 1998. Development of human peripheral TCRBJ gene repertoire. *J. Immunol.* 161:228.

26 Kohsaka, H., Taniguchi, A., Chen, P. P., Ollier, W. E. R. and

Carson, D. A. 1993. The expressed T cell receptor V gene repertoire of rheumatoid arthritis monozygotic twins:rapid analysis by anchored polymerase chain reaction and enzyme-linked immunosorbent assay. *Eur. J. Immunol.* 23:1895.

27 Callahan, J. E., Kappler, J. W. and Marrack, P. 1993. Unexpected expansions of CD8-bearing cells in old mice. *J. Immunol.* 151:6657.

28 Novak, E. J., Liu, A. W., Nepom, G. T. and Kwok, W. W. 1999. MHC class II tetramers identify peptide-specific human CD4^{+} T cells proliferating in response to influenza A antigen. *J. Clin. Invest.* 104:R63.

29 Arden, B., Clark, S. P., Kabelitz, D. and Mak, T. W. 1995. Human T-cell receptor variable gene segment families. *Immunogenetics* 42:455.

30 Williams, A. F., Strominger, J. L., Bell, J., Mak, T. W., Kappler, J., Marrack, P., Arden, B., Lefranc, M. P., Hood, L., Tonegawa, S. and Davis, M. 1993. Nomenclature for T-cell receptor (TCR) gene segments of the immune system. *WHO Bull.* 71:113.